Loop Current ring shedding: the formation of cyclones and the effect of topography.

Laurent M. Chérubin, Yves Morel, and Eric P. Chassignet.

Abstract

The formation of cyclones in the vicinity of the Loop Current ring during the shedding process is analyzed in terms of vortex instability. Using a high resolution ECMWF-daily wind forced MICOM simulation, we show that cyclones are the products of a mixed barotropic-baroclinic vortex instability, which grows around the rim of the Loop Current ring while it is attached to the Loop Current. Cyclones contributes to the separation of the ring from the Loop Current as they grow between them. The QG instability of the Loop Current-like type 'R' vortex shows that a mode 4 baroclinic instability is intensified in the deep layers of the ring while barotropic instability is surface intensified. The nonlinear state shows that a Loop Current-like vortex is indeed a pentapole on an f-plane. On the β-plane, the northern cyclone is separated from the anticyclone by the β-effect and both drift westward. When the topography of the Gulf of Mexico is taken into account, namely the Campeche Bank, the southward slope north of the Loop Current and the Florida shelf east of the Loop Current, several effects are observed: (1) the northern corner of the Campeche Bank erodes the Loop Current ring and its cyclones, and interacts with the vortex most unstable mode; (2) the northern southward slope scatters the northern cyclone while the anticyclone remain coherent and propagate to the west; (3) realistic westward propagation speeds are obtained in the presence of the northern Campeche shelf, which acts as a mirror effect on the Loop Current ring as opposed to the Florida shelf, which tends to block the ring.

1 Introduction

The Gulf of Mexico is a semi-enclosed sea connected to the Caribbean Sea by the Yucatan Channel. The Caribbean Sea carries to the Gulf of Mexico the influence of the western branch of the North Atlantic Subtropical Gyre. The waters of the Caribbean enter the Gulf of Mexico as an intense jet called the Yucatan Current. As the current propagates northward, leaving the Channel and spreading in the southeastern part of the Gulf, it forms the pulsating Loop Current. Finally, the Loop Current leaves the Gulf of Mexico through the Florida Straits, originating the Florida Current, which in turn becomes the Gulf Stream.

Two remarkable processes associated with the Loop Current have been extensively studied, namely its

extensive northward migration into the northeastern Gulf of Mexico continental shelf and the associated shedding of mesoscale anticyclonic rings called Loop Current Rings. The process of separation of warm-core or anticyclonic rings from the Loop Current (originally suggested by Ichiye, 1962) is the most intriguing large scale physical process occurring in the Gulf of Mexico. The mechanism of separation of warm core rings from the Loop Current was first examined in detail by Hurlburt and Thompson (1980, 1982) using numerical model results. In their 2-layer model, they focused on the role of barotropic instability fed by the upper layer kinetic energy and then transferred directly to the Loop Current ring when it pinches off. During the interval between eddy shedding, the model Loop Current did not necessarily meet the necessary instability criterion, so that ring formation time was not determined by an instability growth rate, but rather by the time required for the Loop Current to penetrate into the Gulf and bend to an unstable configuration, at which time an instability grows very rapidly. They found that their model lower layer flow in the vicinity of the Loop Current ring was characterized by a deep cyclone/anticyclone pair, a feature also present in other numerical experiments (Sturges et al., 1993; Welsh, 1996; Inoue, 1998; Welsh and Inoue, 2000).

Surface cyclonic rings are also observed in the Gulf of Mexico. Cochrane (1972) was the first to propose that Loop Current rings could be separated from the Loop Current by cyclonic rings. Elliot (1979) suggested that cyclones observed in the western Gulf were formed along the Loop Current in the eastern Gulf and propagated into the western Gulf during the formation of a Loop Current ring. This scenario was expanded by Vukovich et al. (1979) and Vukovich and Maul (1985). The latter authors speculated that the cold features (the cyclones) intensify through instability processes, thereby leading to the formation below the surface layer of an anticyclone leading to the westward propagation of the cold features in the shear zone between the ring and the Loop Current to the south.

Cyclones were also found to play a role in the separation process in numerical experiments (Hurlburt, 1985, 1986; Wallcraft, 1985, 1986; Oey, 1996). Eddies or meanders were observed to form on the cyclonic shear side of the Loop Current, southwest of its center, and propagate around the Loop. In Hurlburt (1985, 1986), some cyclones nearly reached the outflow port, traveling at 15 km/day, similar to the observational results of Vukovich et al. (1979) and Vukovich and Maul (1985). These cyclonic eddies were formed about every 20 days, but only during a few months prior to an eddy shedding event. In Oey (1996), these cyclones

appear to play a role in Loop Current ring separation (see his Figure 5). However, Oey (1996), as well as Hurlburt and Thompson (1982) and Sturges et al. (1993), also found Loop Current ring separation without resolving frontal eddies in their numerical models.

Satellite data have confirmed the existence of these cyclonic features (also called frontal eddies) along the boundary of a warm core ring. Figure 1 is an example of SSH (Sea Surface Height) maps based on satellite altimetry (Biggs et al., 1996) which shows the Loop Current in necking down position surrounded by three cyclones (blue indicates the lowest sea surface heights). Fratantoni et al. (1998) showed from their observations that Loop Current frontal cyclones are found not only preceding a ring-shedding, but also during the entire extension process. Schmitz (2001) surmised that these frontal eddies may originate from an instability process and possibly amplify and play a role in ring separation. Using an ECMWF-daily forced very high resolution MICOM[1] numerical simulation of the Atlantic Basin, Chérubin et al. (2005) studied the flow patterns in the vicinity of the Loop Current ring during its formation. They observed the generation of strong deep currents underneath the ring, preceding its separation from the Loop Current. These deep current increases in strength were shown to be the consequence of the growth of an instability in the deep part of the Loop Current ring before separation. From the analysis of the growth of the perturbation amplitude and from Flierl's (1988) studies of shielded vortices instability, they concluded that the most unstable modes (m=3, 4) grow in the early stage of the instability growth before the first mode (related to the β-effect) and the elliptical mode (related to the vortex displacement). This high mode instability is a possible explanation for the generation of frontal cyclones (4 or 3) along the boundary of the Loop Current and its triangular shape is observed both in numerical experiments and satellite data (Figure 1).

The following scenario was proposed by Chérubin et al., 2005. The Loop Current ring, which is a shielded vortex (anticyclonic core surrounded by a cyclonic belt), becomes unstable while still connected to the Loop Current (Fig. 2). The vortex instability then produce three of four cyclones at the rim of the anticyclonic core by the cyclonic belt. The cyclones' growth between the Loop Current and the Loop Current ring hence contribute to the separation of the Loop Current ring from the Loop Current. After separation, the Loop Current ring interacts with the topography and propagates westward. The paper is organized as follows: in

[1]Miami Isopycnic Coordinate Ocean Model

section 2, we first examine the characteristics of the instability of a Loop Current ring during a shedding event in the ECMWF-forced MICOM simulation and build a simplified model (by reducing the number of layers) of the Loop Current ring. We then analyze in section 3 and 4, the stability and the nonlinear regimes of this idealized anticyclonic shielded vortex using MICOM in adiabatic mode and focus on the influence of β-effect and topography on the nonlinear growth rate of the most unstable normal mode perturbation. Both the β-effect and topography strongly perturb the nonlinear vortex behavior, and the generation of cyclonic satellites. We also investigate their reciprocal effect on the nonlinear regimes. Conclusions are drawn in section 5.

2 Characteristics of the instability of the Loop Current rings during a shedding event in a high resolution simulation

This section builds upon a very high resolution ($1/12^o$) North Atlantic MICOM simulation that exhibits a realistic circulation in the Gulf of Mexico (Garraffo et al., 2001; Chassignet and Garraffo, 2001; Romanou et al., 2003; Chérubin et al., 2005). MICOM reproduces the most important characteristics of flow in the Caribbean Sea, the Yucatan Channel and the Gulf of Mexico (see Chérubin et al., 2005, for detail). After a brief description of the numerical simulation, the Loop Current ringshedding process is analyzed in terms of potential vorticity anomaly and energy transfers.

2.1 ECMWF daily forced $1/12^o$ MICOM simulation

The fundamental reason for modeling ocean flow in density (isopycnic) coordinates , as it is done in MICOM, is that this system suppresses the diapycnal component of numerically-caused dispersion of material and thermodynamic properties (temperature, salinity, ...) and allows the user to prescribe/parameterize the diapycnal physical processes. This allows isopycnic models to preserve their water mass characteristics and prevents the warming of deep water masses that has been shown to occur in models framed in Cartesian coordinates (Chassignet et al., 1996). The computational domain is the North and Equatorial Atlantic Ocean basin from 28^oS to 70^oN, including the Caribbean Sea, the Gulf of Mexico, and the Mediterranean

Sea. The horizontal grid (6 km on average) is defined on a Mercator projection with resolution given by $1/12^o \times 1/12^o cos(\phi)$, where ϕ is the latitude. The bottom topography is derived from a digital terrain data set with 5' latitude-longitude resolution (ETOPO5). The vertical density structure is represented by 19 isopycnic layers topped by an active surface mixed layer that exchanges mass and properties with the isopycnic layers underneath. The vertical discretization was chosen to provide maximum resolution in the upper part of the ocean. Open ocean boundaries are treated as closed, but are outfitted with 3^o buffer zones in which temperature (T) and salinity (S) are linearly relaxed toward their seasonally varying climatological values (Levitus, 1982), with damping/relaxation time from 5 days at the wall to 30 days at the inner edge of the buffer zone. These buffer zones restore the T and S fields to climatology in order to approximately recover the vertical shear of the currents through geostrophic adjustment. After a six-year spinup with monthly climatological forcing, the model was integrated using surface boundary conditions based on European Centre for Medium-Range Weather Forecasts (ECMWF) daily atmospheric data from 1979 to 1986. The diapycnal mixing consists of a small background value of $1 cm^2/s$ and a Richardson number dependent entrainment parameterization (Papadakis et al., 2003). The high horizontal grid resolution drastically improved the model's behavior in comparison to that of previous coarse-resolution simulations. The major improvements are an excellent representation of western boundary currents (surface and deep) including a correct Gulf Stream separation (Chassignet and Garraffo, 2001) as well as higher eddy activity (Paiva et al., 1999). As mentioned above, the modeled Florida Straits transport is on average $31.4 \times 10^6 \mathrm{m}^3\mathrm{s}^{-1}$ (http://oceanmodeling.rsmas.miami.edu/micom), in line with observations.

2.2 Potential vorticity variations in the Loop Current

We analyze here the potential vorticity anomaly changes of the Loop Current during a ring formation in the MICOM simulation. In the absence of dissipative effects, for each isopycnal layer, potential vorticity is conserved for each particle of the flow (Ertel 1942, Pedlosky 1987) and can be written as:

$$PV = \frac{\zeta + f}{h} \tag{1}$$

where $\zeta = \partial_x v - \partial_y u$ is the relative vorticity, h the thickness of an isopycnal layer, and f the constant Coriolis frequency. It is also useful to define another quantity that we will refer to as the equivalent quasi-geostrophic potential vorticity anomaly (PVA; see Herbette et al., 2003):

$$\begin{aligned} PVA &= H[\frac{\zeta + f}{h} - \frac{f}{H}] \\ &= \frac{H}{h}[\zeta - \frac{f(h-H)}{H}] \end{aligned} \tag{2}$$

$$\tag{3}$$

where H is constant and represents the unperturbed layer thickness. By removing the ambient potential vorticity, the potential vorticity gradients are more clearly seen, and therefore facilitate the study of baroclinic and barotropic instabilities which owe their existence to these potential vorticity gradients (Hoskins et al., 1985). H in the MICOM simulation is provided by the thickness of the layer in the far field from the Loop Current area, which we choose to be west of the Campeche Bank where the disturbance activity is less than elsewhere in the Gulf of Mexico. Layer-by-layer maps of potential vorticity anomaly were computed in the Gulf of Mexico relative to this area. PVA in layer 1 and 4 are displayed in Figure 3 during the northward extension process of the Loop Current. These show that the Loop Current ring is in part surrounded by a belt of positive PVA both at the surface and at depth.

Figure 3a shows that, in the surface layer, the core of the Loop Current has a strong negative potential vorticity anomaly ($\approx -9\ 10^{-5} s^{-}1$). This core is embedded in a belt of less strong potential vorticity anomaly ($\approx -6.5\ 10^{-5} s^{-}1$) surrounded by another belt of positive potential vorticity anomaly. This belt is eventually surrounded by flows of negative potential vorticity anomaly ($\approx -10\ 10^{-5} s^{-}1$). The Charney-Stern theorem (Charney and Stern, 1962) stipulates that the potential vorticity gradients must change sign in or between layers for barotropic or baroclinic instability respectively, to exist. Therefore the horizontal distribution of potential vorticity anomaly in the Loop Current (also observed at depth, Fig. 3b) provides the necessary condition for barotropic instability. In the vertical, the PVA of the core of the Loop Current ring changes sign at 1000 m, as shown in Figure 3c therefore also indicating that the necessary condition for baroclinic instability is satisfied.

We now further analyze the connection between the change of sign of the layerwise PVA and the Loop Current behavior. To provide a picture of the vertical distribution of the PVA, Figure 4 displays the time series of potential vorticity anomaly of layer 2, 6, and 12 over the 6 cycles of ring formation obtained in the ECMWF daily forced MICOM simulation (the shedding events are marked by vertical solid lines). These time series are of the zonal average, at 25^{o}N and between 88^{o}30'W and 83^{o}30'W, of positive and negative potential vorticity anomaly across the Loop Current. In the three layers displayed, each shedding event, is preceded by a long period of high negative potential vorticity anomaly. It is worth noting, in layer 2, that at the end of the third cycle, the slight increase of the negative PVA is associated with the fail of the shedding. The Loop Current Ring reattached the Loop Current. Similarly, the shedding events are also preceded by the sudden increase of the positive potential vorticity anomaly, at the end of the negative potential vorticity anomaly period. The shedding events are therefore dependent on the potential vorticity gradient across the Loop Current.

These results compare well with the observations of Candela et al. (2002) obtained from current measurements in the Yucatan Channel during the CANEK[2] experiment (Ochoa et al., 2001). Indeed, during a period of negative vorticity influx, the Loop Current tends to grow in extension, in area, or in both. During periods of positive influx, the Loop Current retracts and a ring can be shed.

2.3 Energy transfer analysis

In order to estimate the nature of the instabilities and where in the water column they take place, we analyze here the energy transfer time series during the six ring shedding cycles. Hurlburt and Thompson (1982) first showed that barotropic instability was responsible for ring formation in a flat bottom two-layer model. Decreasing the horizontal viscosity of the numerical model in comparison to that of Hurlburt and Thompson's (1982) model, Hurlburt (1985, 1986) analyzed numerical model results for the Gulf of Mexico

[2]The CANEK Project was initiated in December 1996 with the main objective of measuring the exchange flow between the Gulf of Mexico and the Caribbean Sea through the Yucatan Channel. 6 cruises were successfully concluded: December 1996, May 1997, March 1998, January 1999, August 1999 and June 2000. During these cruises extensive shipboard ADCP and CTD/LADCP surveys of the region have been carried out. In August 1999, an 8 mooring array, containing 33 Aanderaa current meters and 8 upward-looking ADCP's, was deployed across the Yucatan Channel, fully recovered in June 2000, and re-deployed for final recovery on June 2001.This research was supported by CICESE, Mexico Rs CONACyT, and the Inter-Americas Institute for Global Change (IAI), and through contracts with Deepstar.

in which cyclonic frontal eddies were present at the rim of the Loop Current. Hurlburt (1985, 1986) found that the Loop Current shedding process was connected with a mixed barotropic-baroclinic instability.

In the MICOM simulation, the total (kinetic and potential) energy and two energy transfers are computed in a box comprising the growing and shedding area of the Loop Current for the six formation cycles. The box longitude ranges from 91^oW to 83^oW and its latitude ranges from 23^oN to 29^oN. The box average eddy kinetic energy and the transfer terms are calculated as expressed by Bleck (1985) and Chassignet and Boudra (1988). Namely, the layerwise transfers of energy from the mean to the disturbance flow are $C(P, K_E)$, the baroclinic conversion, and $C(K_M, K_E)$, the barotropic conversion. Figure 5a shows that the kinetic energy and the potential energy of the perturbation increase just before the shedding events. Figure 5b shows that the baroclinic conversion is toward the mean flow during the Loop Current ring growth (< 0) and then toward the eddy field during the shedding event (> 0). The baroclinic conversion is enhanced in the deep layers of the Loop Current ring. The transfer of kinetic energy from the mean flow to the perturbation increases near the shedding event and decreases in magnitude from layer 1 to layer 9. Overall, baroclinic (barotropic) instability is intensified in the deep (upper) layers of the Loop Current. This result confirms that the shedding events in the MICOM simulation are driven by instabilities and that both baroclinic and barotropic instabilities play a significant role in the separation of the Loop Current ring in agreement with the results of Hurlburt (1985, 1986). In the following section, we will show that the unstable behavior of an idealized Loop Current ring model based on the MICOM horizontal and vertical PVA distribution leads to the formation of cyclones that grow between the ring and the Loop Current (Fig. 2).

3 Instability properties of a shielded vortex on a flat bottom

The horizontal and vertical PVA distribution in the modeled Loop Current and in its vicinity (as described in section 2) are used in this section to build an analytical model aimed at studying the instability of a Loop Current ring-like vortex. The horizontal and vertical distribution of PVA is modeled as shown in Figure 6, with the spatial PVA structure of the Loop Current taken into account. This figure shows a vertical cross section of the Loop Current ring model built upon stripwise constant PVA that will be used for the

quasi-geostrophic (QG) instability study. In the first three layers, the anticyclonic core is surrounded by a cyclonic PVA belt. Based on the vertical PVA profile, the fourth layer of the vortex has a cyclonic PVA. The fifth layer has an infinite depth and no PVA. This type of vortex is called a shielded ring and we study its linear and nonlinear stability in the remainder of this section. Both barotropic and baroclinic instabilities can exist within this idealized vortex in accordance with the Charney-Stern criteria. Impacts of the β-effect and topography are studied in section 4.

3.1 Linear instability

In order to analytically derive the growth rates associated with the above shielded vortex, we need to define an initial profile that is isolated and satisfies the QG approximation. A necessary and sufficient condition for a vortex to be isolated is that the area integral of the relative vorticity ($\zeta = \partial_x v - \partial_y u = \nabla^2 \psi$) vanishes at all depths (Flierl, 1987):

$$\int \int \zeta(x, y, z) dx dy = 0 \tag{4}$$

This condition is pretty much satisfied by the Loop Current ring at the beginning of the shedding process when the anticyclonic core is partially surrounded by a cyclonic belt. To ensure this in our analytical model, we use a continuous power exponential radial profile and annular shielding in the PVA for the first three layers,

$$\begin{aligned} PVA_k &= \Delta Q_k \left(1 - \frac{\alpha}{2} \left(\frac{r}{R}\right)^{\alpha}\right) \exp(-\left(\frac{r}{R}\right)^{\alpha}) \\ & \qquad k = 1, 2, 3 \end{aligned} \tag{5}$$

and a power exponential radial profile only in layer 4,

$$PVA_4 = \Delta Q_4 \exp(-\left(\frac{r}{R}\right)^{\alpha}) \tag{6}$$

where R is the radius of the vortex and ΔQ_k, the maximum PVA in each layer. These profiles are such that the total circulation is zero for any α in each layer (Carton and Legras, 1994).

In the ECMWF-daily forced MICOM simulation described in section 2, the maximum vortex azimuthal speed is $V = 1.5\ cm.s^{-1}$, the vortex radius (outer rim of the cyclonic belt) is $R = 250\ km$ (see Fig. 6, or 200 km if R is the radius of maximum velocity), and the Coriolis parameter at its latitude is $f_0 = 4.2\ 10^{-05} s^{-1}$. This leads to the Rossby number $Ro = 0.14$. Using a density jump of $\Delta\rho/\rho = 6.8\ 10^{-04}$, with the thickness of the first two layers $H = 240\ m$, the Burger number is $Bu = 0.015$. Therefore $Ro/Bu \gg 1$, which does not satisfies the quasi-geostrophic approximation. To estimate the difference between QG and shallow water models in the study of vortex instability, Baey and Carton (2002) analyzed the difference in instability between cyclones and anticyclones in a shallow-water model, which is an effect absent from the quasi-geostrophic model. A noticeable asymmetry appears in their results at small Bu number and in particular, as soon as $Ro/Bu \approx 1$ (i.e., vertical deviations of the density interface are large for the mean vortex). Boss et al. (1996) showed however, that the quasi-geostrophic framework is adequate for describing the instability of a PV front even in regimes where the quasi-geostrophic assumptions are violated.

In the remainder of this subsection, we investigate the Loop Current ring model stability with a $4^{1/2}$-layer quasi-geostrophic analytical model made of piecewise constant strips of PVA. The agreement between the linear instability study results and the nonlinear results (section 3.2) will confirm at posteriori this choice. Finally, since the vortex core is surrounded by a ring of opposite sign PVA, we will refer to this vortex as an "R-vortex" according to the Morel and Mc Williams (1997) classification.

The derivation of the analytical model is given in cylindrical coordinates. The perturbation (or Rayleigh) equations are derived at the PVA front in each layer starting from the relation equation between streamfunction and PVA in QG formalism. The PVA is related to the stream function through the general equation

$$\mathbf{PVA} = \nabla^2 \mathbf{\Psi} + Fr\,\mathbf{\Psi} \tag{7}$$

where $\mathbf{PVA} = [PVA_1, ..., PVA_k, ..., PVA_N]'$, $\mathbf{\Psi} = [\psi_1, ..., \psi_N]$, and Fr is an NxN matrix that is associated with the stretching term. As potential vorticity is assumed piecewise constant, we can thus write:

$$PVA_k = \sum_j \Delta_{k,j} \mathcal{H}(r_{k,j} + \eta_{k,j} - r), \tag{8}$$

where $\mathcal{H}$ is the Heaviside function, $\Delta_{k,j} = Q_{k,j} - Q_{k,j+1}$ is the potential vorticity jump at the jth contour $r = r_{k,j} + \eta_{k,j}(\theta, t)$ in the kth layer, $r_{k,j}$ is the initial radius, and $\eta_{k,j}$ is its deformation. As gradients of Q_k give delta functions, Lagrangian conservation of PVA_k yields

$$\begin{aligned} \frac{D}{Dt} PVA_k &= \sum_j -\Delta_{k,j}\delta(r_{k,j} + \eta_{k,j} - r)\left(\frac{D}{Dt}r - \frac{D}{Dt}\eta_{k,j}\right) \\ &= 0,\ k = 1, ..., N. \end{aligned} \tag{9}$$

Assuming small perturbations of the initial potential vorticity fronts, we can decompose the initial axisymmetric flows as $\psi_{k,j} = \bar{\phi}_k(r) + \phi'_k(r, \theta, t)$, where ϕ'_k is associated with the perturbation. The initial part of the axisymmetric flows $\bar{\phi}_k$ verifies for each layer k

$$\begin{aligned} \nabla^2\bar{\phi}_k + Fr\bar{\mathbf{\Phi}} \mid_k &= \frac{d^2\bar{\phi}_k}{dy^2} + Fr\bar{\mathbf{\Phi}} \mid_k = \sum_j \Delta_{k,j}\mathcal{H}(r_{k,j} - r) \\ & k = 1, ..., N, \end{aligned} \tag{10}$$

from which we derive the angular velocity

$$\bar{\Omega}_k = \frac{1}{r}\frac{d\bar{\phi}_k}{dr}.$$

Linearization of equation (9) gives the Rayleigh equation

$$\frac{\partial}{\partial t}\eta_{k,j} + \bar{\Omega}_k\frac{\partial}{\partial\theta}\eta_{k,j} = -\frac{1}{r_{k,j}}\frac{\partial}{\partial\theta}\phi'_{k,j}. \tag{11}$$

Writing $\eta_{k,j} = \eta_{k,j}\exp(il(\theta - ct))$ and $\phi'_k = \phi'_k(y)\exp(il(\theta - ct))$, ϕ'_k then satisfies the equation

$$\nabla^2\phi'_k + Fr\mathbf{\Phi}' \mid_k = \sum_j \Delta_{k,j}[\mathcal{H}(r_{k,j} + \eta_{k,j} - r) - \mathcal{H}(r_{k,j} - r)] \tag{12}$$

$$k = 1, ..., N, \tag{13}$$

which gives at leading order in the small η limit

$$\nabla^2\phi'_k + (Fr - l^2)\mathbf{\Phi}' \mid_k = \sum_j \Delta_{k,j}\eta_{k,j}\delta(r - r_{k,j}). \tag{14}$$

The last step is to solve equations 8, 9, and 12 for azimuthal mode l. Equations (10) and (12) are similar and their general form can be written

$$\nabla_l^2 \phi_k + Fr\mathbf{\Phi} \mid_k = \Gamma_k \tag{15}$$

with

$$\nabla_l^2 = \frac{1}{r}\frac{\partial}{\partial r} r \frac{\partial}{\partial r} - \frac{l^2}{r^2}.$$

This equation can be solved in terms of vertical modes $P^{(n)} = (P_1^{(n)}, ..., P_k^{(n)}, ..., P_N^{(n)})$ associated with the vortex stretching matrix Fr, so that

$$Fr\mathbf{P} = -D\mathbf{P} \tag{16}$$

where $\mathbf{P} = [P^{(1)}, ..., P^{(N)}]$ is the eigenvector matrix and $D = [\gamma_n^2]$ the diagonal matrix made of the eigenvalues. $R_n = \gamma_n^{-1}$ is the radius of deformation associated with the nth mode. We also define a matrix α, with coefficients $\alpha_k^{(n)}$, so that α is the inverse of the eigenvector matrix $\mathbf{P}$ ($\sum_k \alpha_k^{(m)} P_k^{(n)} = \delta_{nm}$). Thus, if we set

$$\phi_k = \sum_n \phi^{(n)} P_k^{(n)} \quad \text{and} \quad \Gamma_k = \sum_n P_k^{(n)} \Gamma^{(n)},$$

then

$$\Gamma^{(n)} = \sum_l \alpha_l^{(n)} \Gamma_l.,$$

and $\phi^{(n)}$ verifies

$$\nabla_l^2 \phi^{(n)} - \gamma_n^2 \phi^{(n)} = \Gamma^{(n)}. \tag{17}$$

The solution of this equation is obtained from the Green's function for the Helmholtz's operator of the left hand side (see Abramovitz and Stegun, 1972) when $\Gamma^{(n)} = \delta(r' - r)$. The detail of the calculations are given by Vandermeirsch et al. (2001). Thus we obtain the analytical form of the perturbed streamfunction that we use along with the initial axisymmetric flow $\bar{\Omega}_k$, in Eq. (11), which is solved in the normal mode framework. The growth rates of the unstable wavenumber l are the eigenvalues of the system.

We now apply the above derivation to Loop Current ring parameter space. The background stratification is fixed with layer thickness at rest and densities evaluated from the vertical structure of the Loop Current

in the ECMWF-daily forced MICOM simulation. The vortex model numerical values are given in Table 1. The vortex radius is $R = 250\ km$ (rim of the cyclonic belt) and the first internal radius is $Rd = 50\ km$. The vortex potential vorticity anomalies are chosen so that, in each layer, the initial axisymmetric velocity field has realistic extrema at the observed distance in the simulation from the vortex center. Thus $PVA^0 = -4\ 10^{-5}\ s^{-1}$, and the layerwise PV are multiples of PVA^0 as shown in Table 1.

Our vortex is initialized with the PVA profiles (5) and (6), which provide the potential vorticity anomaly jumps and their positions for the linear QG instability model. The parameter α controls the horizontal shear between the anticyclonic core and the cyclonic belt, which is equivalent to specifying the width d (see Fig. 6) of the shield. Flierl (1988), Carton and McWilliams (1989), Carton and Legras (1994), and Baey and Carton (2002), among others, showed the dependence of instability on the vorticity profile controlled here by the steepness parameter α.

Figure 7a shows that mode $m = 4$ is the most unstable mode for this vortex and is triggered when $\alpha \geq 4$. This corresponds to a sufficiently small width of the shield or sufficiently strong horizontal shear. This result agrees with those of Flierl (1988), regarding the growth of high modes for narrow outer shear regions in a two-layer shielded vortex model. Figure 7b displays the amplitude of the resonant PVA fronts (for the front numbering, see Fig. 6). First, this diagram confirms the mixed nature of the vortex instability. Fronts in different layers are resonant (baroclinic instability) and fronts in the same layer are also resonant (barotropic instability). Second, Fig. 7b shows that baroclinic instability is bottom intensified (contours $c5$ and $c7$) while barotropic instability is surface intensified (contours $c1$ and $c2$). This vertical structure agrees with the results obtained in the MICOM simulations (see section 2). We also recover some important properties of shielded vortices found by Saunders (1973) and Flierl (1988), such as the effect of the ratio of the vortex scale to the Rossby radius of deformation. Figure 7c shows that large values of this ratio lead to higher mode instabilities triggered in vortices with narrower outer shear regions.

3.2 Nonlinear evolution and multipoles stability

The nonlinear regimes of the linear vortex discussed in section 3.1 are obtained using the adiabatic version of the MICOM model (Morel, 2001; Jacob et al., 2002; Herbette et al., 2003). The numerical model is

initialized with the same horizontal potential vorticity anomaly profiles as in the analytical study (see (5) and (6)).

The nonlinear steady state of the non-perturbed initialized vortex on an f-plane, for $\alpha = 8$ in layers 1 and 3, is presented in Figure 8. As predicted by the linear instability study, the mode $m = 4$ is the fastest growing for $\alpha = 8$. A pentapole is formed and remains as a long-lived stable multipolar structure. Morel and Carton (1994) showed the existence of dipolar and tripolar stable equilibria for a two-contour Rankine vortex type in 2-dimensional flows. But the stable pentapoles obtained in this study show that more multicomplex multipoles, other than tripoles and quadripoles (Carton and McWilliams, 1989; Carton and Legras, 1994, Baey and Carton, 2002), are stable features of the vortex family in a five-layer shallow-water model. The weak instability does not break the initial circular core of the vortex into smaller vortices. Instead, the potential vorticity rearranges into apparently more stable, axisymmetric, multipolar structures.

4 Interaction of a pentapole with planetary vorticity and topography gradients

The nonlinear state of a Loop Current ring-like vortex was shown in the previous section to be a pentapole on a f-plane. However, planetary vorticity and topography are known to influence the Loop Current ringshedding as discussed by Hurlburt and Thompson , 1982. They showed that the β-effect in their model is responsible for the westward bending of the Loop Current in the Gulf of Mexico as well as for the scale of the eddy and its translation speed. In the presence of sufficient deep water inflow through the Yucatan Channel, the Florida Shelf topography was also shown to occasionally prevent Loop Current penetration, westward bending, and eddy shedding by effectively reducing the port separation, which is the distance between Cuba and the Florida shelf. Bottom topography played another important role by inhibiting baroclinic instability. In this section, we further investigate the combined effects of β and topography on the instability process associated with the separation and propagation of the Loop Current ring.

The area of formation of the Loop Current rings in the eastern Gulf of Mexico is rich in topographic

features that can potentially influence the stability and the propagation properties of oceanic vortices. Three prominent topographic features are worth noting in this area: the Campeche Bank south-southwest of the Loop Current northward extension, the continental southward slope in the northern part of the Gulf, and the western Florida shelf east of the Loop Current (Fig. 9). The Loop Current ring is trapped among these three topographic features during its formation until long after its separation from the Loop Current. Due to differences in shape and position, each of the above mentioned features has a different influence on the Loop Current. The western Florida shelf slope is very abrupt and will be considered in our idealized model of the Gulf of Mexico as a wall. The southward gentle slope of the northern shelf of the Gulf of Mexico can compensate the β-effect in the bottom layers and leave the eddy less perturbed. Finally, the Campeche bank can actually act as a large amplitude perturbation on the Loop Current ring during its formation.

4.1 Influence of the β-effect on a pentapole

Section 3 demonstrated that the vortex instability of a Loop Current-like ring yields to the formation of a pentapole on an f plane. On a β-plane, however, the stability problem cannot be as clearly posed since the initial vortex is not anymore a steady solution. There it combines with the propagation dynamics, which contribute to axial asymmetry. As shown by Dewar and Killworth (1995) and Morel and McWilliams (1997), there is a tendency for the development of a mode 1 perturbation to be induced by the β-effect. The influence of β can be strong enough so that the end product of the instability can be quite different from that on the f-plane.

Figure 10 presents the nonlinear states of on a β-plane of the same eddy described in subsection 3.2 for the f-plane (Fig. 8, $\alpha = 8$). The β-effect causes the development of a secondary cyclonic circulation, north of the anticyclone, as the result of the mode 1 perturbation on the initial shielded vortex. Dewar and Killworth (1995) showed a similar behavior in their study of oceanic ring stability based on the influence of deep corotating and counterrotating currents. Their study showed that oceanic eddies with counterrotating deep flows are more unstable than those with corotating deep flows and therefore more sensitive to the β effect. The end product of their nonlinear instability on a β-plane (most unstable mode $m = 2$) was also the formation of a cyclonic circulation north of the initial vortex. In our simulation, the nonlinear state

changes from an horizontal dipole to a more turbulent state in which the anticyclone is split by cyclones as the whole moves to the west as a consequence of the β-effect. As a result of the interaction between the mode 1 forced by β and the mode 4, the most unstable mode is changed to mode 3. The perturbation grows on the rim of the shielded vortex with a strong asymmetry in the cyclones' strength and the splitting and filamentation are enhanced. The higher mode instability interaction with β-effect breaks the coherence of a vortex with corotating deep flows.

4.2 Influence of the Campeche Bank on a pentapole on an f-plane

In the southern Gulf of Mexico, the Campeche Bank extends at depths between 200 and 500 m for 280 km northward of the Yucatan Peninsula coast (Fig. 9). The underwater northern tip of the Campeche Bank is relatively sharp and drops within 50-100 km to 3000 m depth. The shape and the slope of the Campeche shelf act as a subsurface cape on the Loop Current ring as it grows in the basin-like area defined by the north-east shelf of the Campeche Bank, the north coast of Cuba, and the western Florida shelf.

In order to estimate the influence of the Campeche Bank shape on the Loop Current rings, the Bank is modeled as either a circular or an elliptic subsurface cape with a linear sloping shelf. The influence of the shelf slope and the relative position of the subsurface cape to the Loop Current ring are better studied on an f-plane with the center of the vortex positioned north of the cape. If the subsurface cape is wide enough, as a finite amplitude perturbation of mode 1 type, the subsurface cape perturbation interacts with the mode 4 ring perturbation, yielding a mode 3 perturbation growing on the ring (Fig. 11). For narrow subsurface capes (not illustrated), higher mode perturbations are forced and smaller scale cyclones and filaments are generated. The difference in shape of the subsurface cape induces a difference in the erosion of the vortex on the slope via filamentation. The erosion of the vortex will also depends on its proximity to the subsurface cape (Herbette et al., 2003). Sharp subsurface capes (i.e., elliptic) produce less filamentation of the vortex core than wide subsurface capes (i.e., circular). In both the elliptic and circular cases, the subsurface cape introduces an asymmetry in the distribution of the cyclones with the strength of the cyclones increasing with the slope of the shelf as shown in Figure 11. Advection of water by the vortex off the slope , on the western side of the vortex, off the slope, generates cyclonic vorticity, by conservation of potential vorticity.

The size of these anomalies depends on the magnitude of the shelf slope. They are larger for steep slopes and increase vortex splitting.

4.3 Combined effect of the Campeche Bank and of the continental southward sloping bottom on a pentapole

In this subsection, we investigate the influence of the continental southward sloping bottom located north of the Loop Current ring in the Gulf of Mexico. The results are analyzed in term of cyclone population around the anticyclonic core, as this is the main product of the instability and topography interaction process. Figure 12 shows the differences in cyclone population and intensity in layer 3 for several configurations.

Jacob et al. (2002) showed that a considerable reduction in the eddy propagation speed can be induced by a southward linear slope that opposes the β-effect in the bottom layer. Moreover, the decay of the eddy was found by Jacob et al. (2002) to be much slower than in the case with only β-effect and the eddy retained its strength over a longer period of time. For the idealized Loop Current ring case and in the absence of β, the ring ends up drifting to the east on the southward slope as shown in Figure 12a. The erosion of the vortex by filamentation is therefore reduced since it moves away from the Campeche Bank (elliptic shape to minimize the erosion of the vortex on the slope).

The competition between β and the steepness of the slope is illustrated in Figure 12b-c. In the case of the steepest linear slope experiment (Fig. 12b), the anticyclonic ring is more strongly sheared by the cyclone population when compared to an experiment with a slope not as steep (Fig. 12c). With the decrease in slope steepness, filamentation of the deep anticyclone is as strong and the cyclone interaction with the anticyclone is less effective. The shape of the slope also matters: the influence of the cyclones was found to be smaller with an exponentially varying slope (Fig. 12d) than with a linear southward slope experiment since the cyclones are further away from the anticyclone. The dispersion of the cyclonic belt by topographic Rossby waves is found to be weaker in the absence of β (Fig. 12a). Furthermore, the anticyclonic core is found to remain coherent despite the fact that Thierry and Morel (1999) showed that large rings (radius $> 100km$) become unstable on very steep slope and are dispersed by topographic Rossby waves.

Let's now look at the surface signature of the vortices (Fig. 13). Thierry and Morel (1999) and Jacob et al. (2002) found that steep slopes increase deep eddy flow scattering by topographic Rossby waves and weaken the deep part of vortices, increasing their sensitivity to filamentation and splitting. The anticyclone is indeed found to interact more with the surrounding cyclones (Fig. 13a) as it is weakened by the steep southward linear topography. When scattering is not as strong in the lower layer, the anticyclone is more coherent than when the southward slope is steep (high scatter) and the anticyclone-cyclone interaction is not as strong (Fig. 13b). In presence of an exponentially sloping bottom (Fig. 13c), the bottom slope effect changes meridionally. Cyclones, north of the anticyclone, are more dispersed than the anticyclone. The anticyclone retains its strength longer, while the cyclones quickly weaken. Therefore the interaction of the anticyclone with the cyclone is also reduced. With no southward slope and with β, the anticyclone-cyclone interaction is strong, and the anticyclone is eroded and split by the cyclone and by the Campeche Bank in the deep layers. Only the cyclone keeps its initial strength (not shown).

In summary, the upper layer anticyclone behaves like the lower one in terms of interaction with the cyclone and production of filaments. It is worth noting that the filaments are produced in the deep layers (below 300 m), where the vortex core leans on the Campeche Bank slope. Vortex stretching induces filament signatures in the surface layer (Fig. 13), but the vortex width remains larger than in the deep layers.

4.4 Additional effects of the Campeche Bank north shelf and of the West Florida shelf

Various westward propagation speeds are obtained for the idealized configurations described so far. The observations suggest that the westward zonal drift should be between 2 and 5 km/day (Coats, 1992; Elliott, 1982; Shay et al., 1998; Schmitz, 2001). The Loop Current ring drift in the high resolution MICOM simulation with values on the order of 4 km/day shows a good agreement with the observations. However, the idealized Loop Current rings in the above experiments do not move as fast, therefore suggesting that the β effect alone may not be sufficient to account for the westward drift ofLoop Current rings as it has been surmised (Hurlburt and Thompson, 1982). The importance of the continental southward slope on the westward drift is illustrated in Figure 14 for experiments where the Campeche bank is represented as half of

an ellipse pointing to the north and where the vortex is initialized north of the tip of the cape.

With no β-effect and $h_b^0 = 3030$ m, the displacement is actually to the east. With β-effect and the same slope, the eddy drift remains small since the bottom slope mostly cancels the β-effect in the bottom layer. The westward drift increases as the bottom slope is decreased ($h_b^0 = 2500$ m), but the eddy is still in contact with the Campeche cape after 150 days. With an exponential slope, the zonal drift is increased: the ring core is ≈ 400 km away from its initial position after 150 days, instead of 250 km away with a linear slope.

When the northern shelf of the Campeche Bank is added to the west of the cape, the westward propagation speed is strongly increased, and realistic propagation speeds corresponding to the average speed observed in observations and realistic numerical models are obtained. Moreover, the deep anticyclone separates completely from the cape and drifts westward along the Campeche shelf (Fig. 13d). This increase in the translation speed can be explained by the mirror effect of the coast on the vortex. The northern topography of the Campeche Bank acts as a wave guide that increases the anticyclone advection to the west. Without the Campeche shelf, when the vortex is initialized east of the cape, the motion to the west is blocked and erosion on the Campeche cape creates filaments and splitting of the anticyclone. The presence of the northern Campeche shelf west of the cape contributes to the passage of the ring west of the cape (Fig 14e, thick dotted line). As in the realistic MICOM simulation (Fig. 14g, triangles), the propagation speed is slow in the vicinity of the cape and increases toward the west of the cape.

Addition of the Florida shelf actually reduces significantly the drift of the vortex for both types of continental slopes, but much less for a linear slope than for an exponential one. As the distance d between the Campeche Bank eastern shelf and the Florida shelf decreases, trapping of the anticyclone-cyclone dipole increases. To maintain a reduced influence of the Florida western shelf, a distance $d > R$ is necessary.

It is worth noting that in all the experiments described above, more than one cyclone is observed north of the anticyclone. But in all cases, there is always one cyclone that also drifts westward north of the anticyclone, forming a horizontal dipole with the anticyclone both in the deep and surface layers (Figs. 12 and 13), as observed in other numerical simulations (Sturges et al., 1993; Oey, 1996; Murphy et al., 1999;

Chérubin et al., 2005).

5 Summary and conclusions

Observations based on satellite SSH maps and numerical modeling show the presence of cyclones in the vicinity of the Loop Current ring, from before its separation from the Loop Current until its decay in the western Gulf. In this study, we focused on the origin of the cyclones in the vicinity of the Loop Current ring before the separation from the Loop Current itself. Using the ECMWF daily forced North Atlantic very high resolution MICOM simulation as a benchmark experiment, we confirmed that the separation of the Loop Current ring and the generation of cyclones in its vicinity were the consequence of an instability (Chérubin et al., 2005). The present study shows that the instability is mixed: barotropic instability is surface intensified while baroclinic instability is bottom intensified. Each of the shedding events in the MICOM simulation is associated with an increase of the potential vorticity anomaly gradient across the vortex. The core becomes more negative while on the rim of the vortex, a positive anomaly grows. This particular feature allows us to classify this vortex as a shielded or 'R' vortex (Flierl, 1988, Morel and McWilliams, 1997), which provides us with their instability properties: higher unstable modes grow as the width of the shield decreases. The linear instability study showed that mode 4 is the most unstable mode of a Loop Current ring-like vortex and the nonlinear regime evolved in a steady pentapole on a f-plane.

We then investigated the interaction of the Loop Current-like vortex with the β-effect, which transforms the vortex into an unstable quadripole as the result of the interaction between mode 4 and mode 1, the latter being forced by the planetary vorticity gradient. The cyclonic ring of the vortex is separated from the anticyclone and both propagate westward as a dipole, the cyclone being north of the anticyclone.

When a topographic feature equivalent to the submarine promontory of the Campeche Bank, south-southwest of the Loop Current ring, is added, filamentation and vortex splitting are enhanced by the submarine cape. Filamentation increases with the width and slope of the cape. The cape acts as a finite amplitude perturbation, which interacts with the most unstable mode of the vortex. The generation of cyclones varies with the size of the cape. Besides the cape effect, due to the β-effect, the main cyclone is formed north of

the anticyclone. The strength of the cyclone contributes to the anticyclone splitting.

In the presence of a southward slope north of the vortex, scattering of the northern cyclone and of the anticyclone is increased in the deep layer. It has a visible signature in the surface, and the steepness of the slope controls the westward propagation speed of the anticyclone. Since the cyclone is north of the anticyclone, the strength of the cyclone is decreased by scattering more than the strength of the anticyclone. The latter remains coherent and propagates faster to the west. Changing the slope profile, from linear to exponential, increases the northern cyclone scattering by topographic Rossby waves. The anticyclone interacts less with the cyclones and travels faster to the west. This result reveals the crucial role of the southward slope north on the Loop Current.

The presence of the northern shelf of the Campeche Bank increases the westward propagation of the anticyclone by adding the velocity component of its mirror effect of the coast and by adding the fast velocity component of the westward propagation of topographic Rossby waves. This shelf was also shown to favor the crossing of the cape by the anticyclone when its initial location was east of the cape. The Campeche northern shelf also compensates the blocking effect of the western Florida shelf.

The MICOM simulation indeed confirms that the anticyclone follows the 1000 m depth contour of the Campeche shelf until it interacts with the western Gulf circulation (Fig. 15a). This result is indeed obtained in most Gulf of Mexico numerical simulations (Hurlburt and Thompson, 1980; Sturges et al., 1993; Oey, 1996; Murphy et al., 1999; Welsh and Inoue 2000), but was never noticed. The propagation speed in the idealized numerical model and in the MICOM simulation is in the range of the observed speeds (2-5 km/day), with an average (observed) of 4km/day. The MICOM simulation also shows the pervasive role and presence of cyclones both at the surface and in the deep layers. Besides the northern cyclone that forms, with the anticyclone, a feature that was called a 'modon' in previous model results (Sturges, 1993; Oey, 1996; Murphy et al., 1999; Welsh and Inoue 2000), more cyclones surround the anticyclone during its formation and its propagation to the west, especially in the deep layers as observed in the idealized model. Finally, SSH maps from the Real-Time Altimetry project at the Colorado Center for Astrodynamics Research show the Loop Current ring following the 1500 m contour isobath, confirming the above results (Fig. 15 b and c).

In summary, this study shows the generation of cyclones by the Loop Current ring instability before separation. The growth of cyclones between the Loop Current and the ring most likely contributes to their separation at the surface as in the deep layers, as shown by the MICOM simulation.

6 Acknowledgments

The study is supported by the Mineral Management Service under contracts # 1435-01-00-CT-31076 and 01-99-CT-31028 (via SAIC) and by NSF grant # OCE 03-271808. The authors thank Professors W.J. Schmitz Jr. and W. Sturges for fruitful discussions and contributions to this paper. They also thank L. T. Smith for careful reading and editing of the manuscript.

7 Bibliography

Abramovitz, M., and I. Stegun, 1972. *Handbook of Mathematical Functions.* DOver, 1046 pp.

Baey J-M., and X. Carton, 2002. Vortex multipoles in two-layer rotating shallow-water flows. *J. Fluid Mech.*, **460**, 151-175.

Bleck, R., 1985. On the conversion between mean and eddy components of potential and kinetic energy in isentropic and isopycnic coordinates. *Dyn Atmos. Oceans*, **9**, 17-37.

Biggs, D.C., G.S. Fargion, P. Hamilton and R.R. Leben, 1996. Cleavage of a Gulf of Mexico loop current eddy by a deep water cyclone. *J. Geophys. Res.*, **101**, 20,629-20,641.

Boss, E., N., Paldor, and L. Thomson, 1996. Stability of a potential vorticity front: from quasi-geostrophy to shallow-water. *J. Fluid. Mech*, **315**, 65-84.

Candela, J., J. Sheinbaum, J.L. Ochoa, A. Badan and R. Leben, 2002. The potential vorticity flux through the Yucatan Channel and the Loop Current in the Gulf of Mexico. *Geophys. Res. Lett.*, **29**, (22), 2059, doi:10.1029/2002GL015587.

Carton, X.J., and B. Legras, 1994. The life-cycle of tripoles in 2D incompressible flows. *J. Fluid Mech.*, **267**, 53-82.

Carton, X.J., and J.C. McWilliams, 1989. Barotropic and baroclinic instabilities of axisymmetric vortices in a QG model. In J.C.J. Nihoul and B.M. Jamart (eds), *Mesoscale/Synoptic Coherent Structures in Geophysical Turbulence*, Elsevier Oceanographic Series, **50**, 225-244.

Charney, J.G., and M.E. Stern, 1962. On the instability of internal baroclinic jets in a rotating atmosphere. *J. Atmos. Sci.*, **19**, 159-172.

Chassignet, E.P., and D.B. Boudra, 1988. Dynamics of Agulhas retroflection and ring formation in numerical model. Part II. Energetics and ring formation. *J. Phys. Oceanogr.*, **18**, 304-319.

Chassignet, E.P. and Z.D. Garraffo, Viscosity parameterization and the Gulf Stream separation. In "From Stirring to Mixing in a Stratified Ocean", P. Muller and D. Henderson, Eds., Proceedings of 'Aha Huliko'a Hawaiian Winter Workshop (January 15-19), 37–41, U. of Hawaii, 2001.

Chassignet, E.P., L.T. Smith, R. Bleck, and F.O. Bryan, 1996. A model comparison: numerical simulations of the North and Equatorial Atlantic oceanic circulation in depth and isopycnic coordinates. *J. Phys. Oceanogr.*, **26**, 1849-1867.

Chérubin L.M., W. Sturges, and E.P. Chassignet, 2005. Deep flow variability in the vicinity of the Yucatan Straits from a high-resolution MICOM simulation. *J. Geophys. Res.*, in press.

Coats, D.A., 1992: The Loop Current, J.D. Milliman and E. Imamura (eds.), In the Physical oceanography of the U.S. Atlantic and Eastern Gulf of Mexico, U.S. dept of the Interior, Mineral Management Service, Atlantic OCS Region, Herndon, Va., Chapter 6.

Cochrane, J.D., 1972: Separation of an anticyclone and subsequent developments in the Loop Current (1969), L.R.A. Capurro and J.L. Reid (eds.), In Contributions on the physical oceanography of the Gulf of Mexico, Gulf Publishing Co., Houston, Texas, 91-106.

Dewar, W.K., and P.D. Killworth, 1995. On the stability of oceanic rings. *J. Phys. Oceanogr.*, **25**, 1467-1487.

Elliot, B.A., 1979. *Anticyclonic rings and the energetics of the circulation of the Gulf of Mexico.* PhD Dissertation, Texas A & M Univ., College Station, TX, 188pp.

Elliott, B.A., 1982: Anticyclonic rings in the Gulf of Mexico. *J. Phys. Oceanogr.*, **12**, 1292-1309.

Ertel, H., 1942. Ein neuer hydrodynamischer Wirbelsatz (A new scaler to characterize hydrodynamic eddies. *Meteor. Z.*, **59**, 271-281.

Flierl, G.R., 1987. Isolated eddy models in geophysics. *Annu. Rev. Fluid Mech.*, **19**, 493-530.

Flierl, G.R., 1988. On the instability of geostrophic vortices. *J. Fluid. Mech.*, **197**, 349-388.

Fratantoni D.M., T.N. Lee, G.P. Podesta and F. Muller-Karger, 1998. The influence of the Loop Current perturbations on the formation and evolution of Tortugas eddies in the southern Straits of Florida. *J. Geophys. Res.*, **103**, 24759-24779.

Garraffo, Z.D., A.J. Mariano, A. Griffa, C. Veneziani and E.P. Chassignet, 2001. Lagrangian data in a high-resolution numerical simulation of the North Atlantic I, Comparison with in situ drifter data, *J. Mar. Sys.,* **29**, 157-176.

Herbette, S., Y. Morel, and M. Arhan, 2003. Erosion of a surface vortex by a seamount. *J. Phys Oceanogr.*, **33**, 1664-1679.

Hoskins, B.J., McIntyre,M.E., and A.W. Robertson, 1985. On the use and significance of isentropic vorticity maps. *Q. J. R. Met. SOc.*, **111**, pp. 877-946.

Hurlburt, H.E., and J.D. Thompson, 1980. A numerical study of loop current intrusion and eddy shedding. *J. Phys. Oceanogr.*, **10**, 1611-1651.

Hurlburt, H.E., and J.D. Thompson, 1982. The dynamics of the Loop Current and shed eddies in a numerical model of the Gulf of Mexico. In Hydrodynamics of semi-enclosed Seas, Amsterdam, New York: Elsevier. J.C.J. Nihoul(ed.), 243-298.

Hurlburt, H.E., 1985. Cyclonic eddy generation in the Gulf of Mexico. In: *Proceedings of the sixth annual Gulf of Mexico information transfer meeting*, sponsored by Department of the Interior Minerals Management Service, Gulf of Mexico OCS regional Office, text 272-273, figure p. 283.

Hurlburt, H.E., 1986. Dynamic transfer of simulated altimeter data into subsurface information by a numerical ocean model. *J. Geophys. Res.*, **91**, 2372-2400.

Ichiye,T., 1962. Circulation and water-mass distribution in the Gulf of Mexico. *Geofisica Internl.*, **2**, 47-76.

Inoue, M., 1998. Modeling deep water in the Gulf of Mexico. An appendix in: *Workshop on environmental issues surrounding deepwater oil and gas development.* Final report, compiled by R.S. Carney, OCS MMS 98-0022. U.S. Dept. of the Interior, Minerals Management Service, Gulf of Mexico OCS region, New Orleans, La., 163pp.

Jacob, J.P., E.P. Chassignet, and W.K. Dewar, 2002. Influence of topography on the propagation of isolated eddies. *J. Phys. Oceanogr.*, **32**, 2848-2869.

Levitus, S., 1982. *Climatological Atlas of the World Ocean.* NOAA professional paper no. 13, U.S. Government Printing Office, Washington D.C., 173 pp.

Morel, Y., and X.J. Carton , 1994. Multipolar vortices in two-dimensional incompressible flows. *J. Fluid. Mech.*, **267**, 23-51.

Morel, Y., and J. McWilliams, 1997. Evolution of isolated interior vortices in the ocean. *J. Phys. Oceanogr.*, **27**, 727-748.

Murphy, S.J., and H.E. Hurlburt, 1999. The connectivity of eddy variability in the Caribbean Sea, the Gulf of Mexico, and the Atlantic Ocean. *J. Geophys. Res.*, **104**, (C1), 1431-1453.

Oey, L.Y., 1996.Simulation of mesoscale variability in the Gulf of Mexico: sensitivity studies, comparison with observations, and trapped wave propagation. *J. Phys. Oceanogr.*, **26**, 145-175.

Paiva, A.M., J.T. Hargrove, E.P. Chassignet, and R. Bleck, 1999. Turbulent behavior of a fine mesh (1/12°) numerical simulation of the North Atlantic, *J. Mar. Sys.*, 307-320.

Papadakis, M.P., E.P. Chassignet, and R.W. Hallberg, 2003. Numerical simulations of the Mediterranean Sea outflow: Impact of the entrainment parameterization in an isopycnic coordinate ocean model, *Ocean Modelling*, **5**, 325-356.

Pedlosky, J., 1987. *Geophysical Fluid Dynamics.* Springer-Verlag, 710 pp.

Romanou, A., E.P. Chassignet, and W. Sturges, 2003. The Gulf of Mexico circulation within a high-resolution numerical simulation of the North Atlantic. *J. Geophys. Res.*, **109**, C01003, doi:10.1029/2003JC001770.

Saunders, P.M., 1973. The instability of a baroclinic vortex. *J. Phys. Oceanogr.*, **3**, 61-65.

Schmitz, W.J., Jr, 2001. On the circulation in and around the Gulf of Mexico. Vol. I: A review of the deep water circulation. http//www.cbi.tamucc.edu/gomcirculation/

Sturges, W., J.C. Evans, S. Welsh and W. Holland, 1993. Separation of warm core rings in the Gulf of Mexico. *J. Phys. Oceanogr.*, **23**, 250-286.

Shay, L.K., A. J. Mariano, S.D. Jacob, and E. H. Ryan, 1998. Mean and Near-Inertial Ocean Current Response to Hurricane Gilbert. *J. Phys. Oceanogr.*, **28** (5), 858-889.

Thierry, V. and Y. Morel, 1999. Influence of a strong bottom slope on the evolution of a surface-intensified vortex. *J. Phys. Oceanogr.*, **29**, 911-924.

Vandermeirsch, F., Y. Morel and G. Sutyrin, 2001. The net advective effect of a vertically sheared current on a coherent vortex. *J. Phys. Oceanogr.*, **31**, 2210-2225.

Vukovich, F.M., B.W. Crissman, M. Bushnell and W.J. King, 1979. Some aspects of the Gulf of Mexico using satellite data and in-situ data. *J. Phys Oceanogr.*, **9**, 1214-1222.

Vukovich, F.M., and G.A. Maul, 1985. Cyclonic eddies in the eastern Gulf of Mexico. *J. Phys. Oceanogr.*, **15**, 105-117.

Welsh, S.E., 1996. A numerical modeling study of the Gulf of Mexico under present and past environmental conditions. PhD Dissertation, Louisiana State Univ., Baton Rouge, La., pp206.

Welsh, S.E., M. Inoue, 2000. Loop Current rings and the deep circulation in the Gulf of Mexico. *J. Geophys. Res.*, **105**, C7, 16,951-16,959.

Wallcraft, A., 1985. Gulf of Mexico circulation modeling study, year 1. Progress report by JAYCOR, submitted to the Minerals Management Service, Metairie, LA., Contract No. 14-12-0001-30073.

Wallcraft, A., 1986. Gulf of Mexico circulation modeling study, year 2. Progress report by JAYCOR, submitted to the Minerals Management Service, Metairie, LA., Contract No. 14-12-0001-30073.

layer	Layer thickness	ρ $(kg.m^{-3})$	ΔQ
1	$H_1 = 150\ m$	$\rho_1 = 1023.81$	$\Delta Q_1 = 0.6\Delta Q_0$
2	$H_2 = 50\ m$	$\rho_2 = 1025.06$	$\Delta Q_2 = \Delta Q_0$
3	$H_3 = 500\ m$	$\rho_3 = 1025.64$	$\Delta Q_3 = 0.6\Delta Q_0$
4	$H_4 = 250\ m$	$\rho_4 = 1026.05$	$\Delta Q_4 = -0.06\Delta Q_0$
5	$H_5 = 4000\ m$	$\rho_5 = 1046.05$	$\Delta Q_5 = 0$

Table 1: Physical parameters of vortex model.

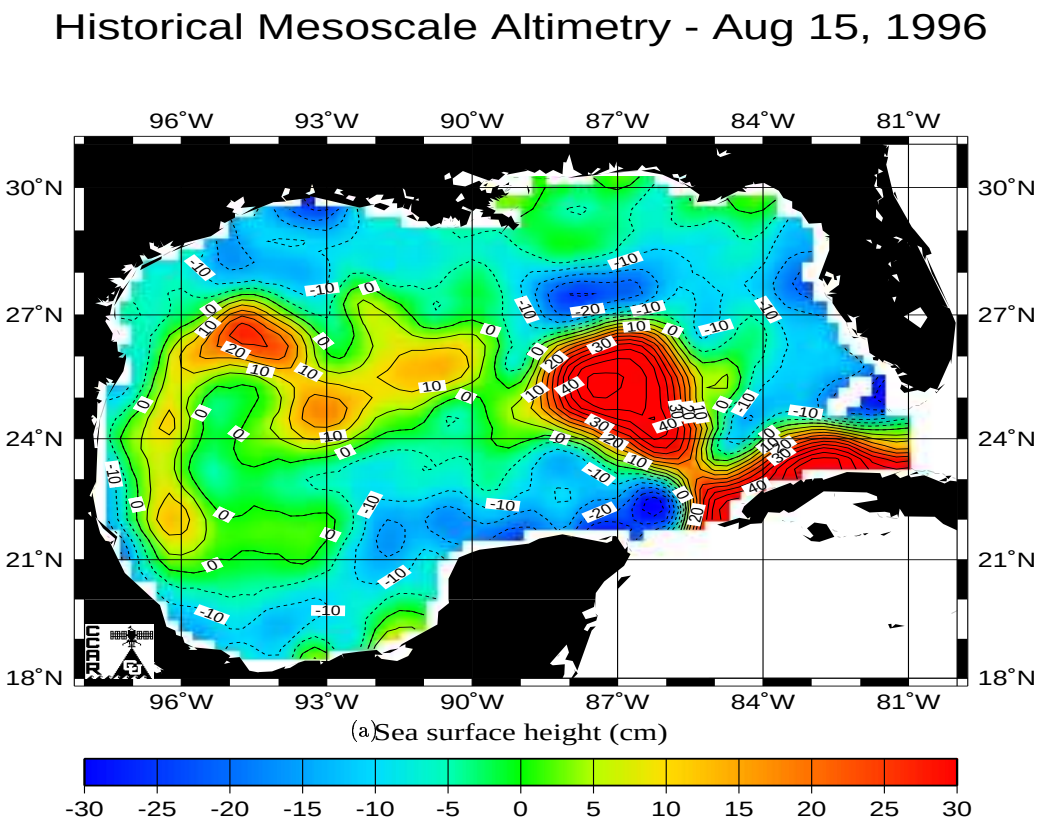

Figure 1: Sea Surface Height (SSH, August 15, 1996) map of the Gulf of Mexico from the Real-time altimetry project at the Colorado Center for Astrodynamics Research. Blue (red) indicates the lowest (highest) sea level.

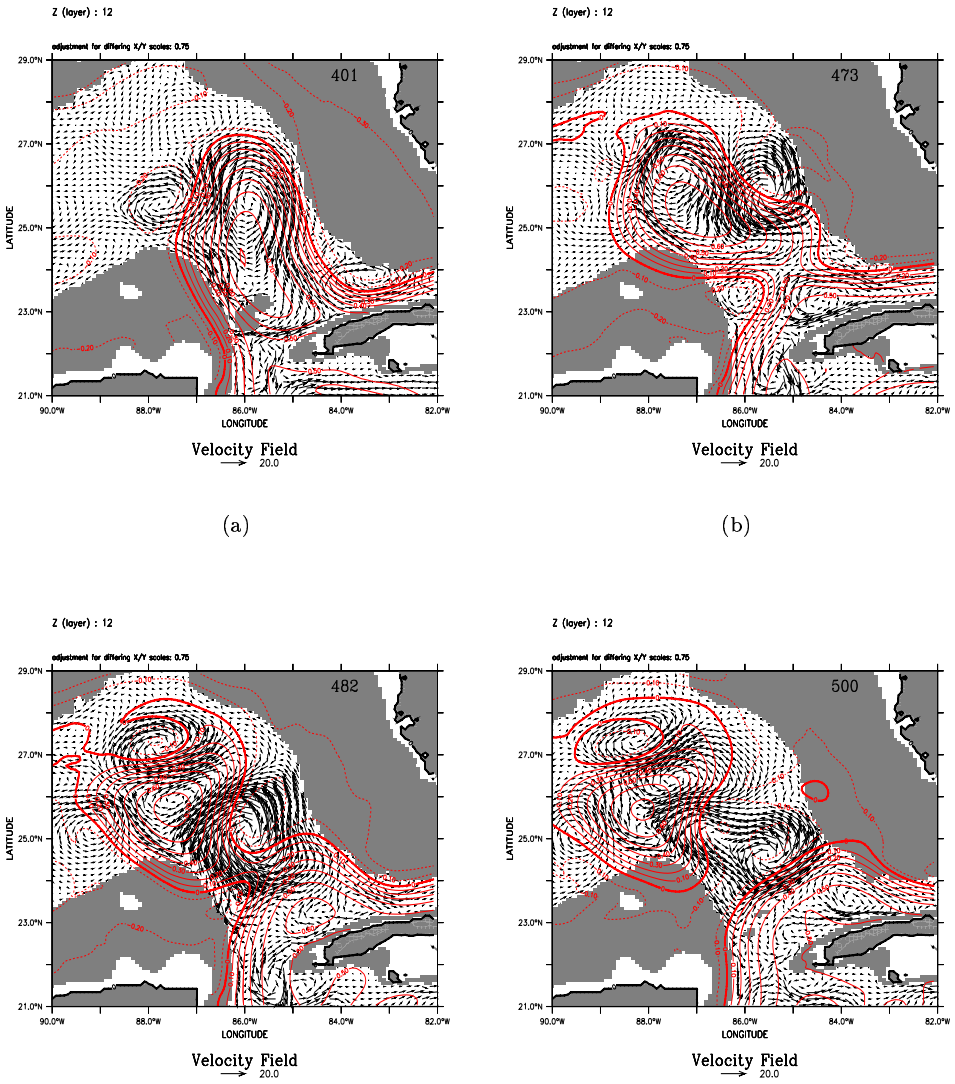

Figure 2: (a) - (d) frame sequence of the flow circulation in MICOM layer 12 superimposed on the Sea Surface Height (red contours in meters). Solid lines are positive contours. The gray shading corresponds to the bottom topography mask. The number in the caption is the day. The scale (cm/s) of the arrows is given by the vector length just below the frame (from Chérubin et al., 2005).

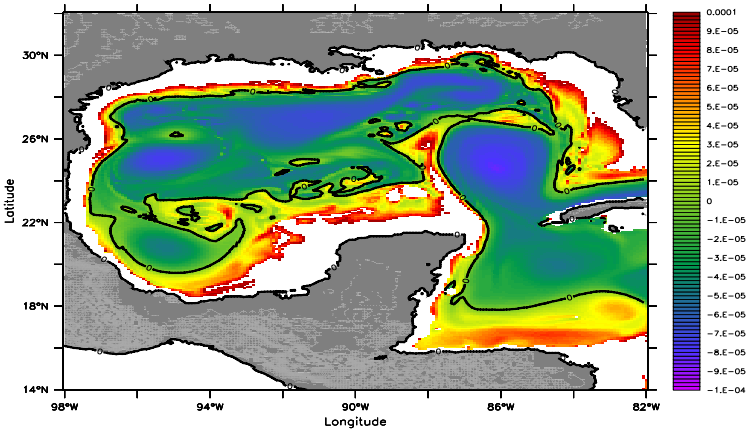

(a)

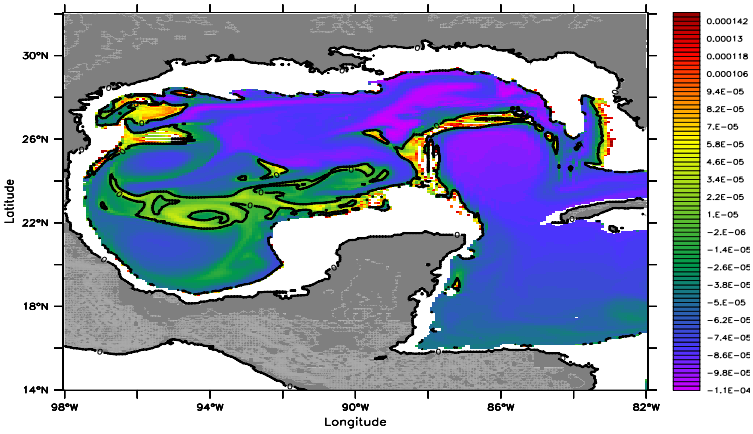

(b)

Figure 3: (a) and (b) are the maps of potential vorticity anomaly in the MICOM North Atlantic high resolution simulation before the a Loop Current ring shedding event. Violet (red) indicates strong negative (positive) anomalies. The black contour shows the change of sign of the potential vorticity anomaly. (a) layer 1 of the model; (b) same as (a) in layer 4.

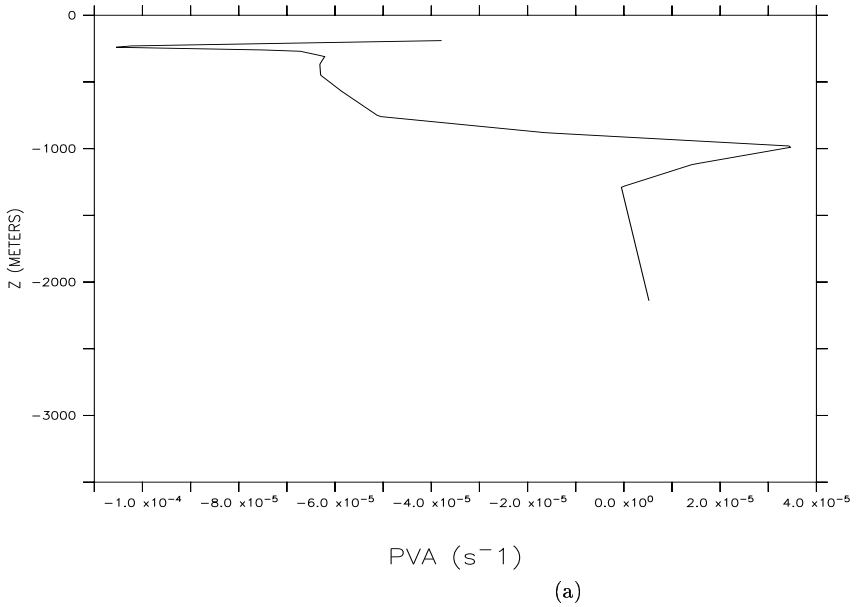

(a)

Figure 3: continued; (c) is the potential vorticity anomaly vertical profile in the Loop Current.

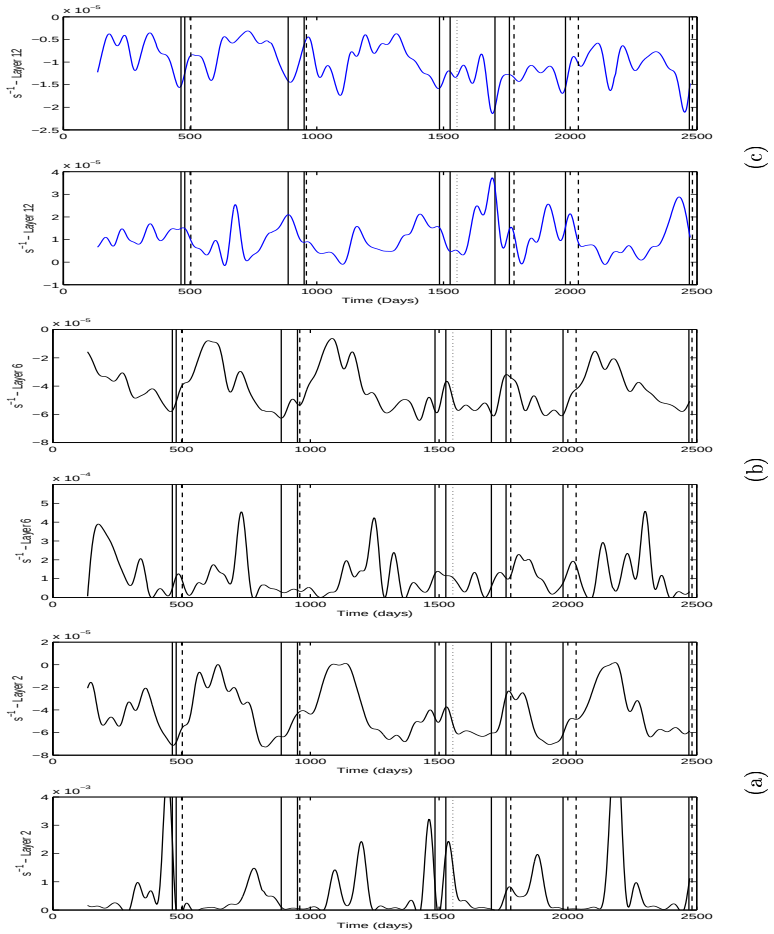

Figure 4: Time series of potential vorticity anomalies from the MICOM North Atlantic high resolution simulation. These time series cover the 6 integral ring shedding events and are series of the zonal average, at 25^{o}N and between 88^{o}30'W and 83^{o}30'W, of positive and negative potential vorticity anomalies across the Loop Current. Each separation is marked by a vertical solid line. The dashed line marks the end of the cycle (see also Chérubin et al., 2005). (a) layer 2; (b) layer 6; (c) layer 9.

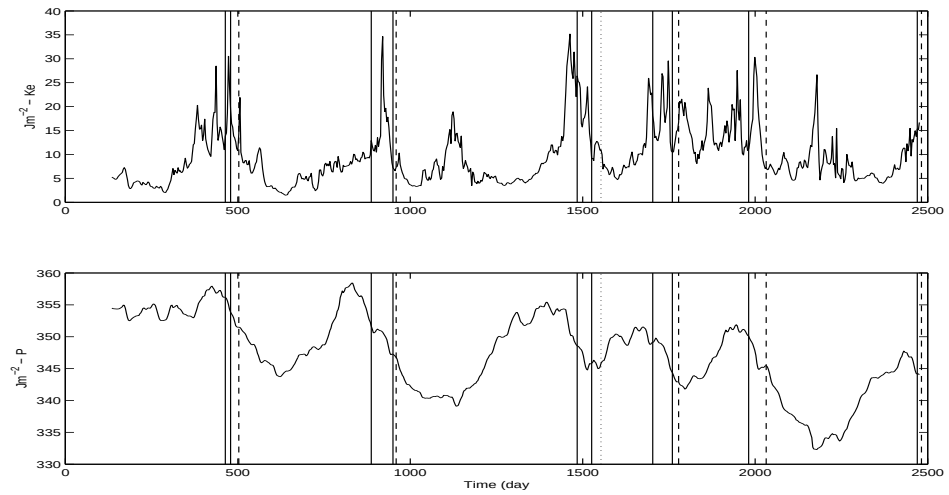

(a)

Figure 5: Time series of the kinetic energy (upper panel), and potential energy (lower panel) from MICOM simulation

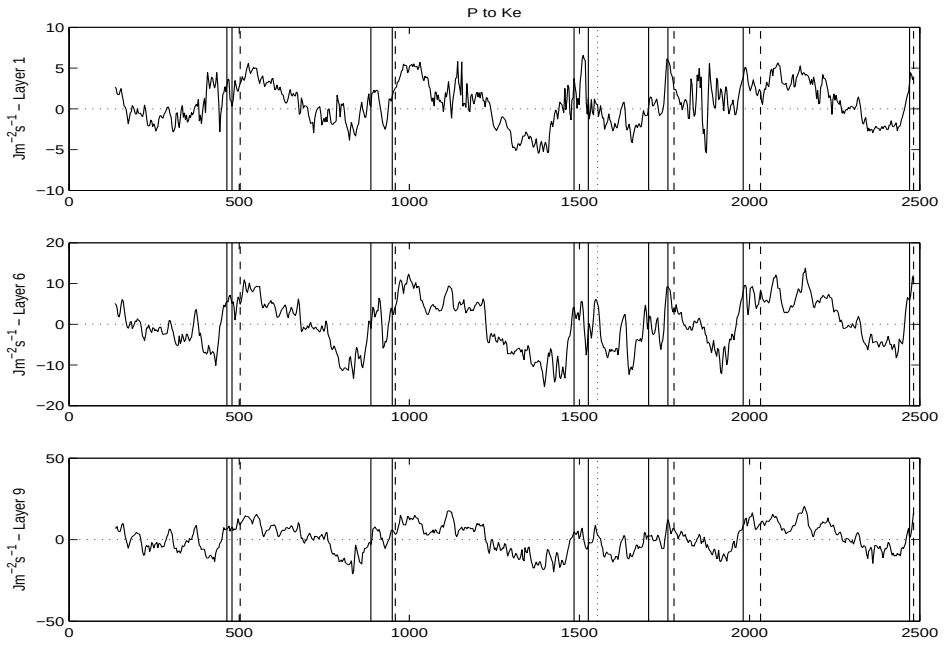

(a)

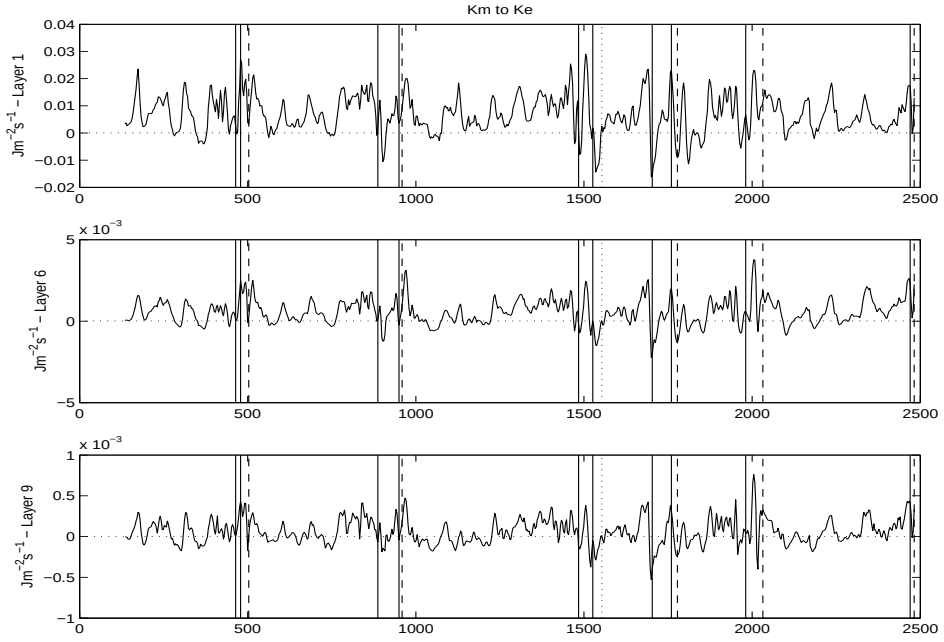

(b)

Figure 5: continued; (b) Baroclinic conversion term $\mathrm{C}(P, K_E)$ for, from top to bottom, layers 1, 6, and 9. (c) Mean flow - perturbation kinetic energy transfer $\mathrm{C}(K_M, K_E)$ for the same layers as in (b).

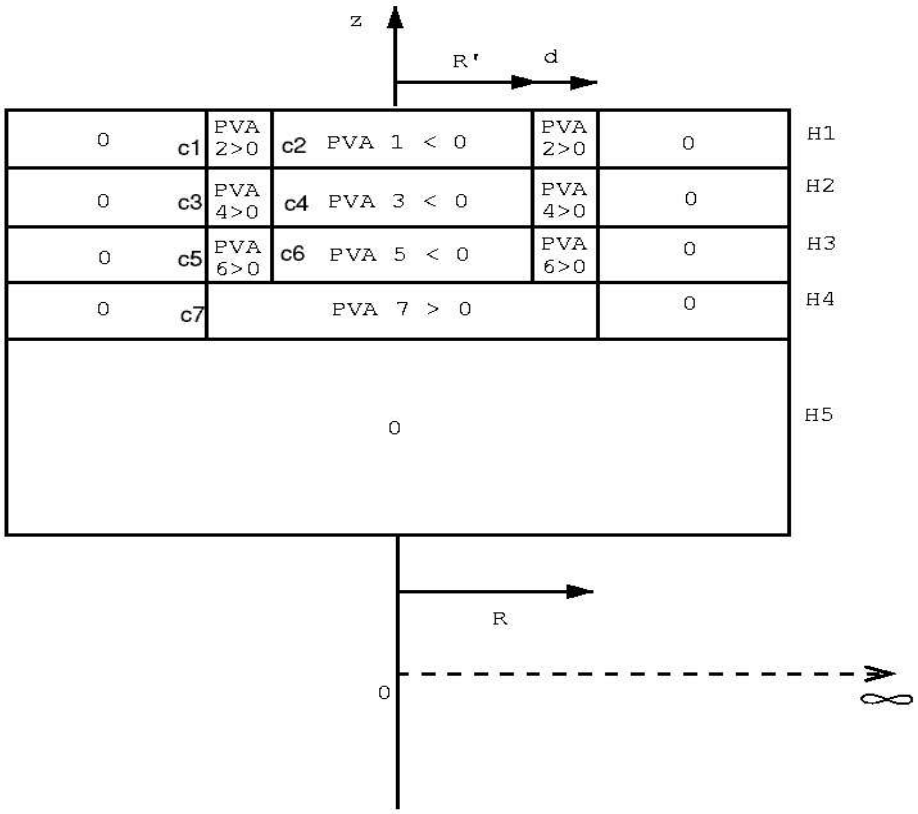

Figure 6: Cross section of the QG Loop Current ring model used for the analytical study. Two circular PVA contours are defined per layer in the first three layers. The inner (outer) contour is around the anticyclonic (cyclonic) core (belt). Only one circular contour is define is layer 4. PVA contours are labeled cj where j is the contour number. R is the vortex radius defined here by the external rim of the cyclonic belt. d is the width of the cyclonic belt. R' is the radius of the inner core. Hi, i=1:5, is the layer thickness.

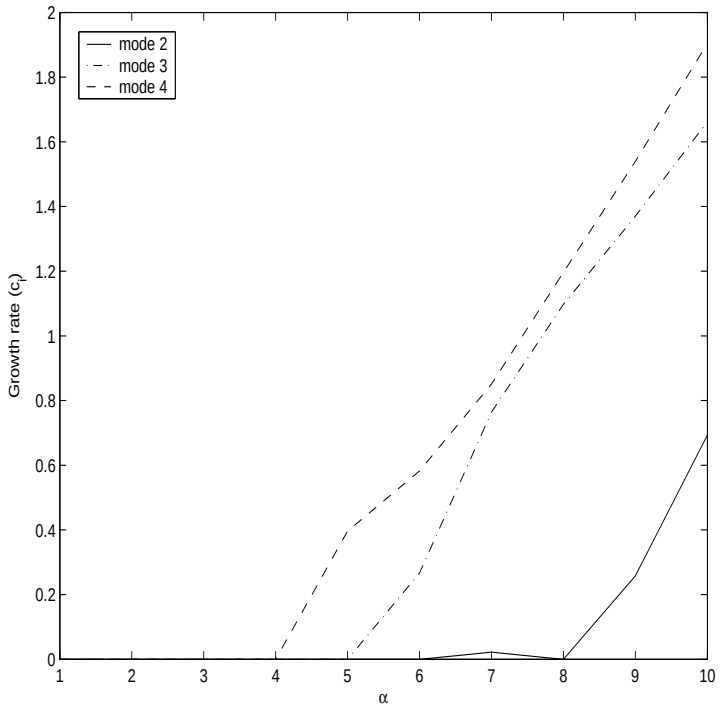

(a) Figure 7: Growth-rates of unstable modes 2, 3, and 4 as a function of α.

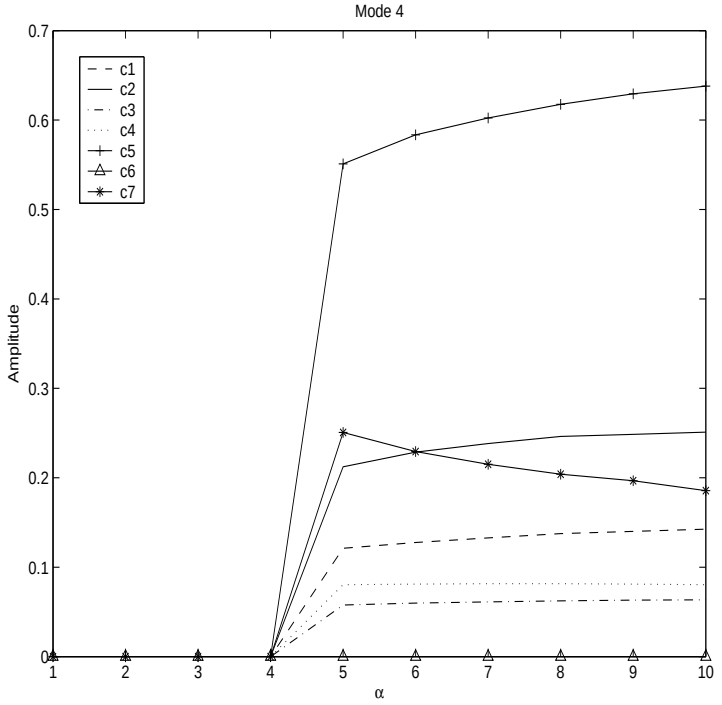

(b)

Figure 7: (a) growth-rates of unstable modes 2, 3, and 4 as a function of α. (b) amplitude of the perturbation on the potential vorticity fronts (see Fig. 3 for their numbering).

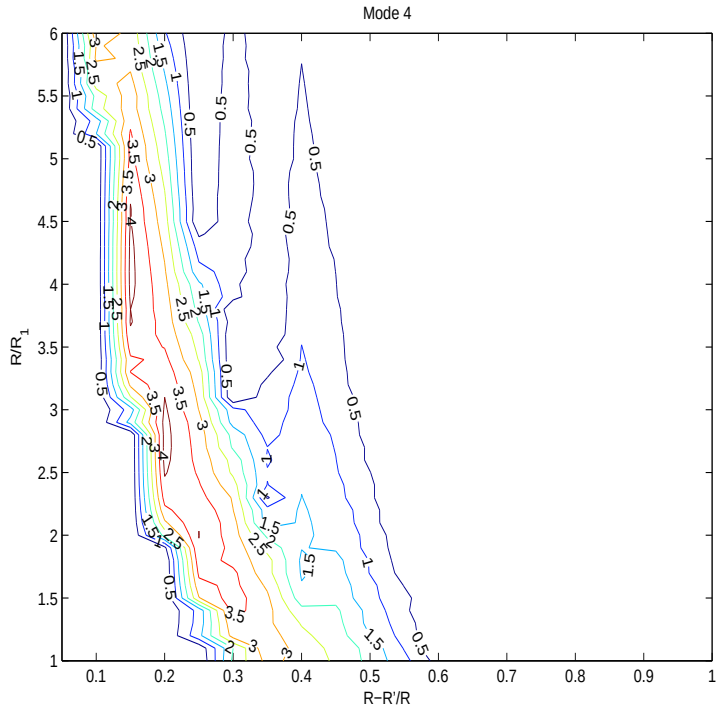

(a)

Figure 7: continued; (c) growth rate diagram as a function of the radii ratio between the outer and inner contours $(R - R'/R)$, and as a function of the ratio between the first Rossby radius R_1 and the vortex radius R.

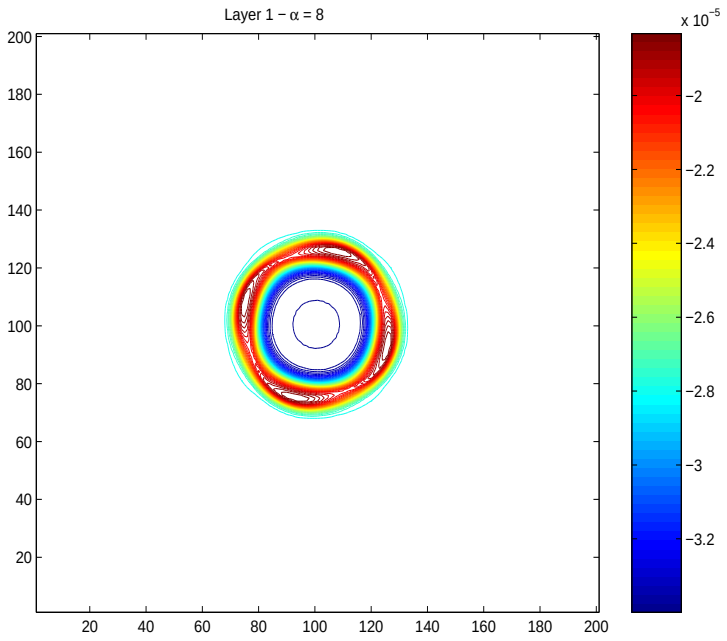

(a)

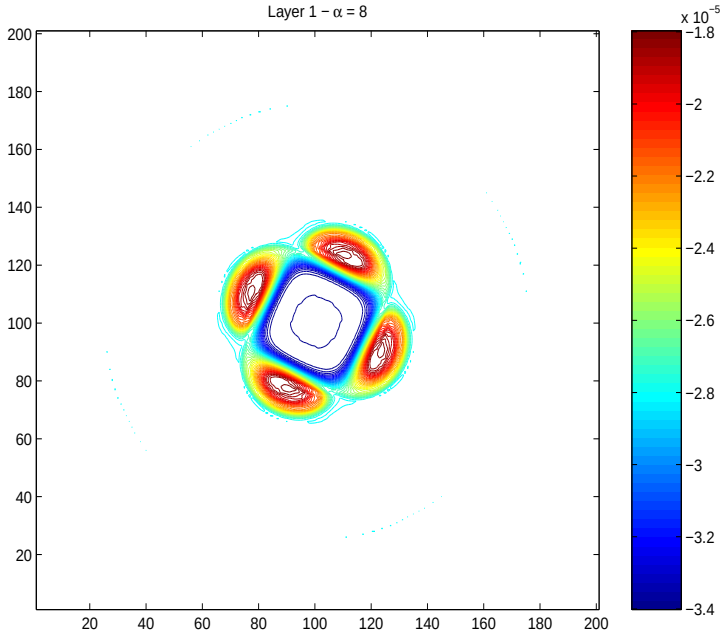

(b)

Figure 8: PVA contours of the idealized model of the Loop Current ring showing the formation of a stable pentapole on an f-plane in layers (a, day 25 & b, day 50).

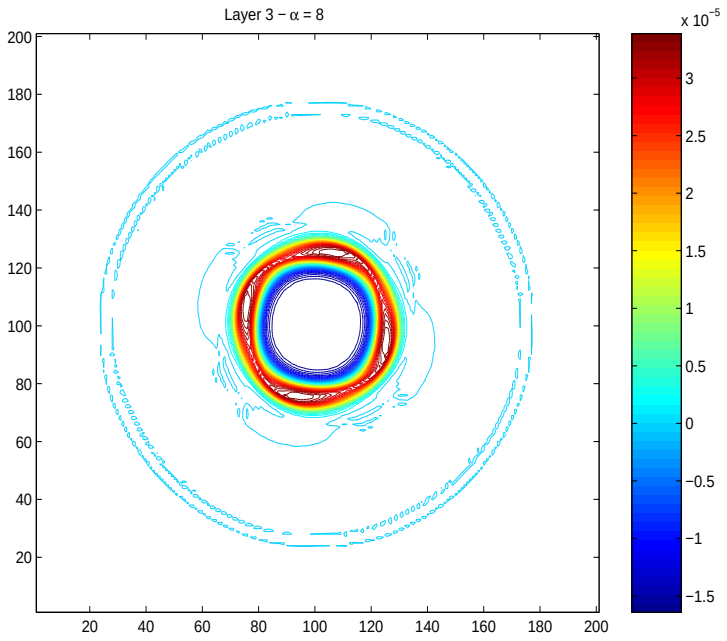

(a)

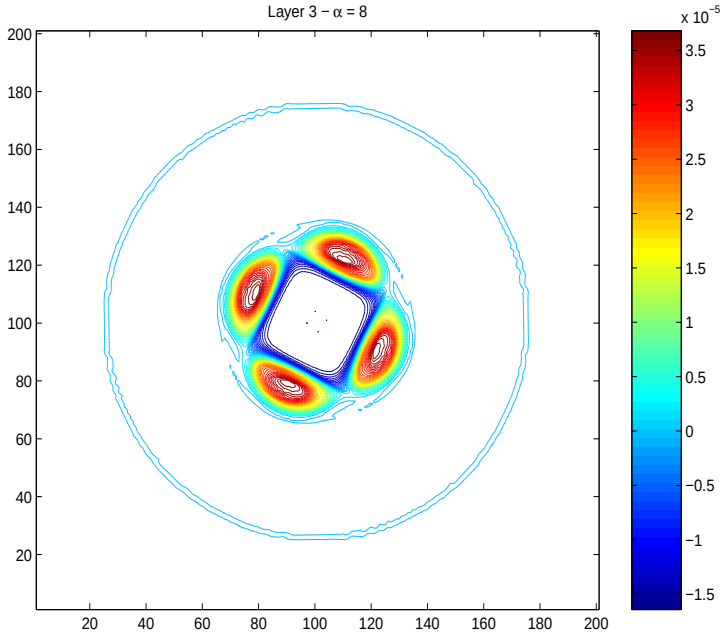

(b)

Figure 8: continued; PVA contours of the idealized model of the Loop Current ring showing the formation of a stable pentapole on an f-plane in layer 3 (c & d) for the same days as in layer 1.

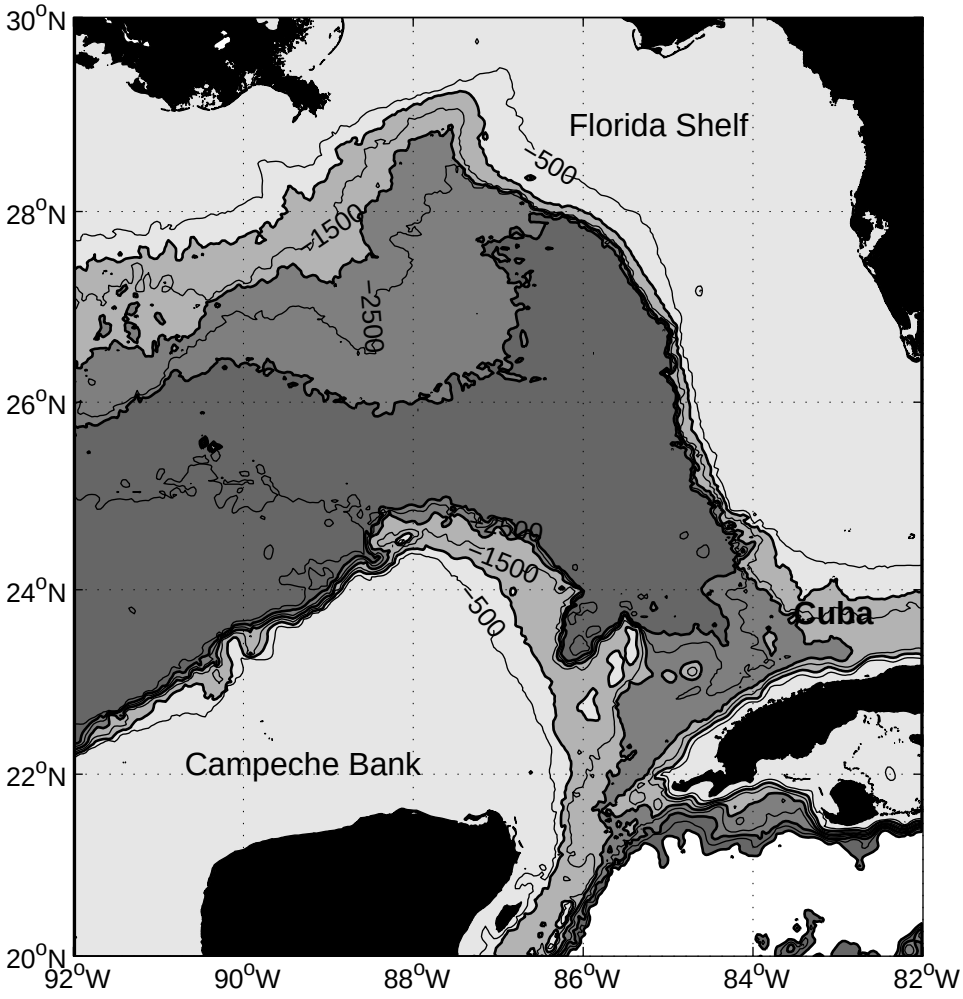

Figure 9: Bottom topography of the Gulf of Mexico

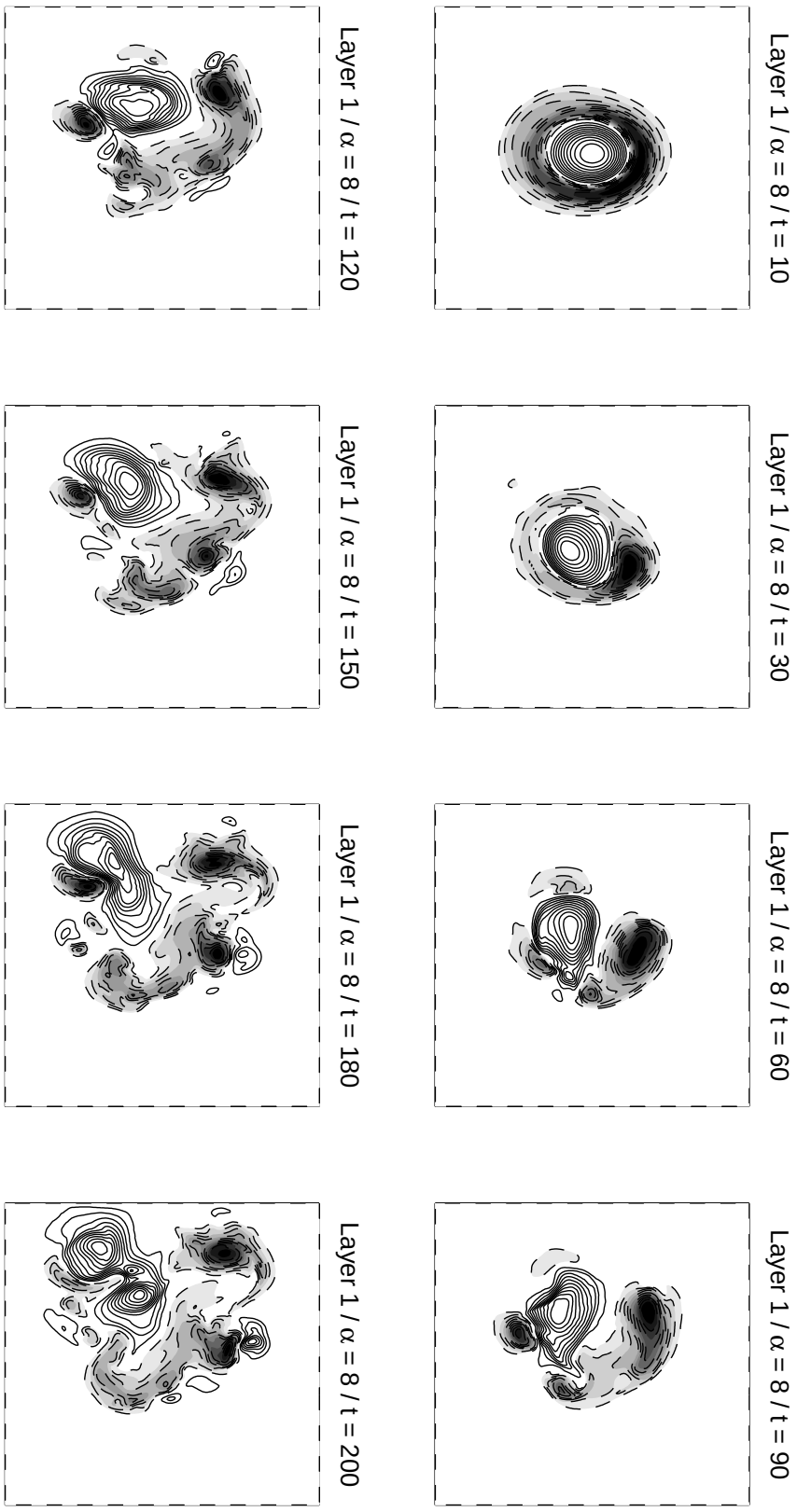

Figure 10: Layer 1 thickness anomaly contours showing the nonlinear evolution of a pentapole on a β-plane. Solid line contours correspond to positive thickness anomalies and dashed and shaded contours correspond to negative thickness anomalies.

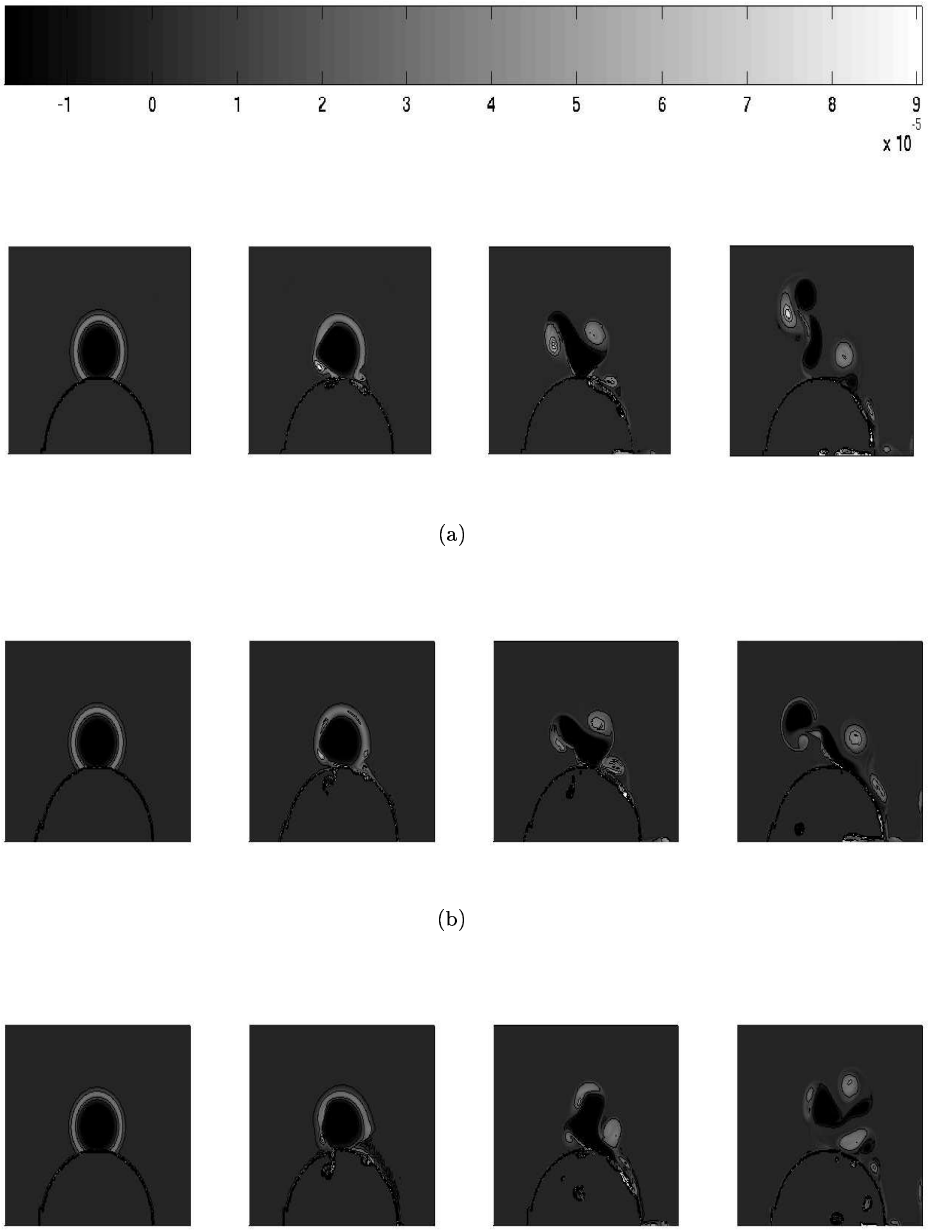

(a)

(b)

(c)

Figure 11: Time evolution of the potential vorticity anomaly in layer 3 of the Loop Current ring numerical model for days 1, 10, 30, and 60 (from left to right). Negative potential vorticity anomalies are contoured. The three panels, from (a) to (c) show the effect of decreasing the slope width of the circular 'Campeche Bank' on the ring: (a) vertical wall; (b) 100 km wide; (c) 200 km wide.

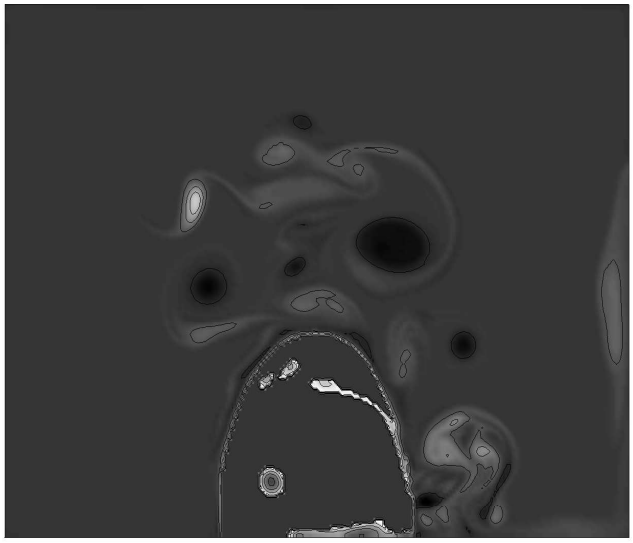

(a)

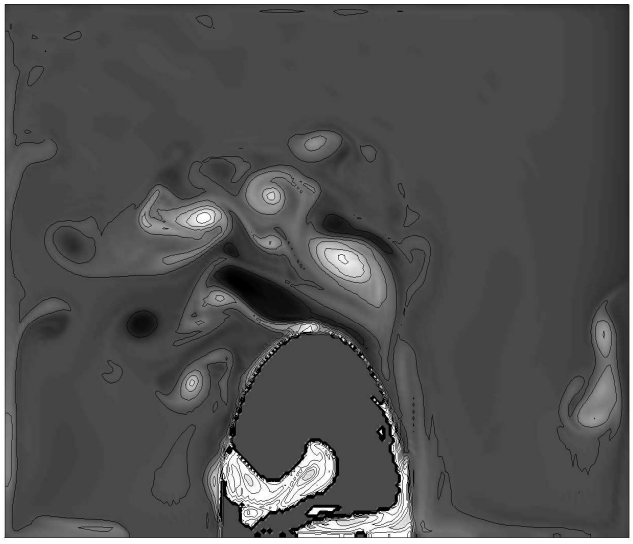

(b)

Figure 12: Potential vorticity anomaly in the Loop Current ring model layer 3, at day 130, with no β-effect, with $h_b^0 = 3030\ m$, and a linear bottom slope (a). (b) same as (a) with β-effect.

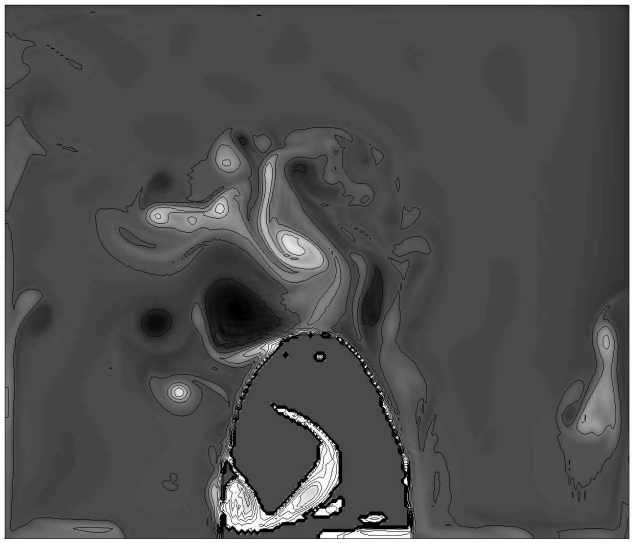

(a)

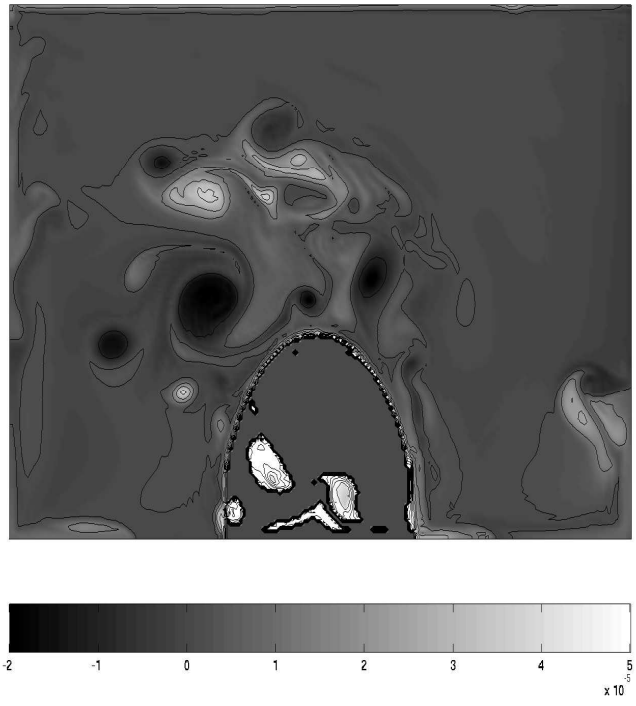

(b)

Figure 12: continued; potential vorticity anomaly in the Loop Current ring model layer 3, at day 130, with β-effect and $h_b^0 = 2500\ m$, and a linear bottom slope (c). (d) same as (c) with $h_b^0 = 4650\ m$, and an exponential bottom slope.

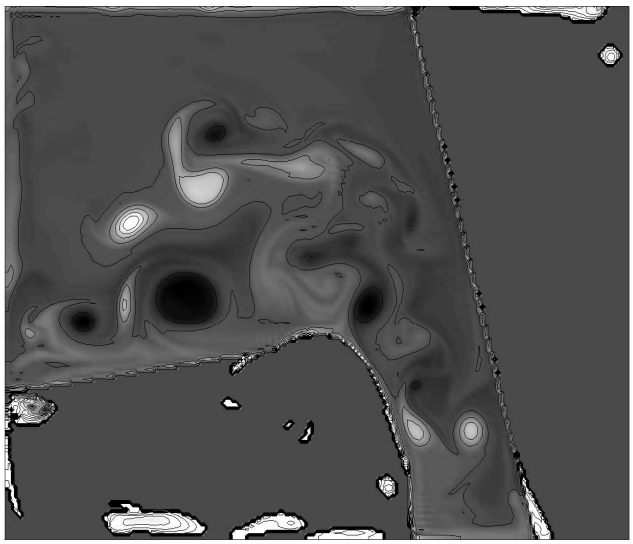

(a)

Figure 12: continued; (e) exponential bottom slope with Campeche and Florida shelves experiment.

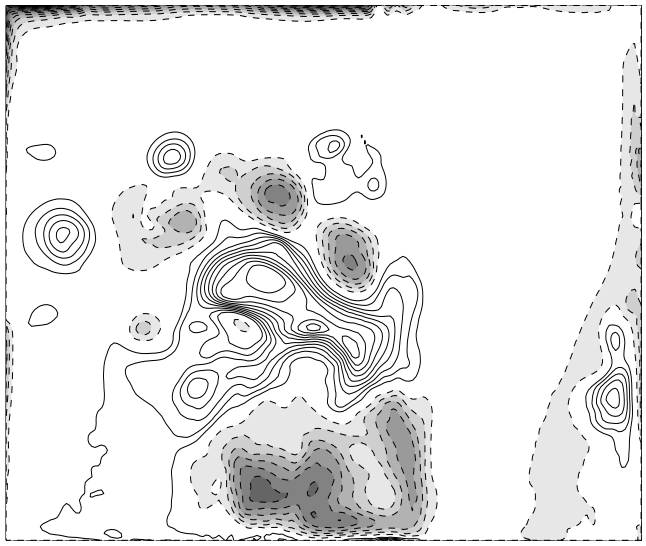

(a)

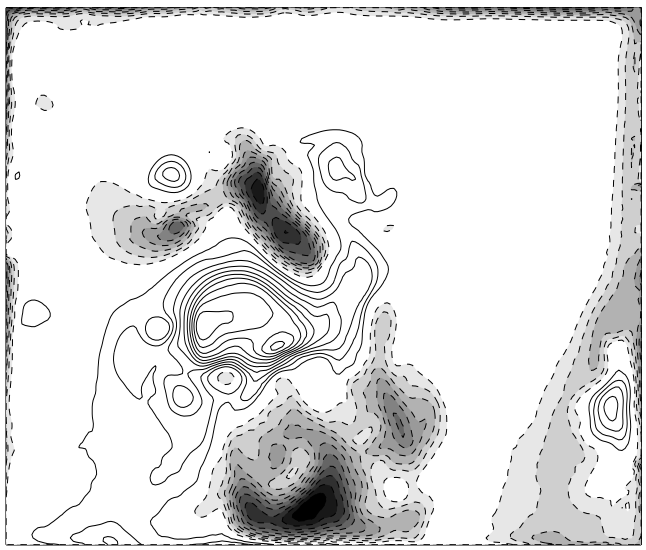

(b)

Figure 13: Layer 1 thickness anomaly at day 130 for various bottom slopes with β-effect and $h_b^0 = 3030\ m$ (a). (b) same as (a) with $h_b^0 = 2500\ m$. Positive (negative) values are contoured (shaded and dashed line).

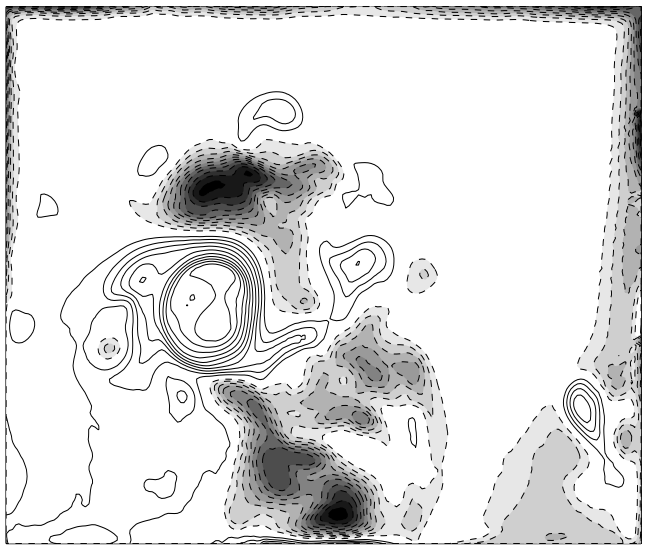

(a)

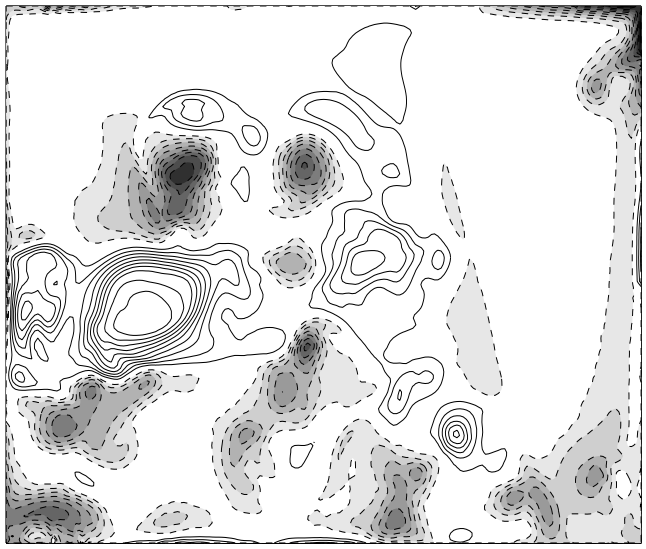

(b)

Figure 13: continued; (c) exponential bottom slope with $h_b^0 = 4650\ m$. (d) exponential bottom slope with Campeche and Florida shelves experiment.

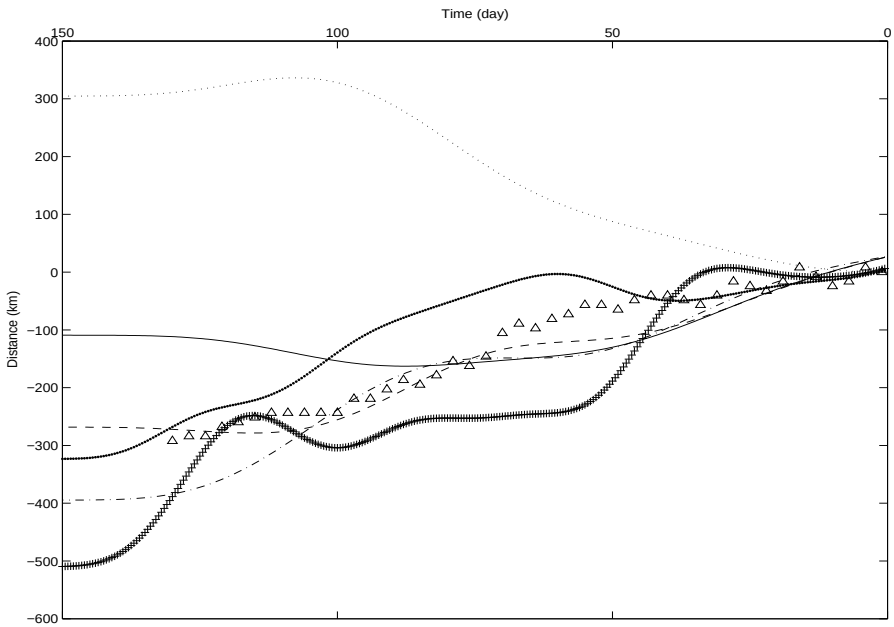

Figure 14: Anticyclone center displacement (km) versus time (day). (a) dotted line, no β-effect, and $h_b^0 = 3030\ m$. For all the other trajectories, β-effect is present. (b) solid line, $h_b^0 = 3030\ m$. (c) dashed line, $h_b^0 = 2500\ m$. (d) dashed-dotted line, exponential slope with $h_b^0 = 4650\ m$. (e) thick dotted line, same exponential slope as in (d) with Campeche northern shelf and the initial vortex east of the cape. (f) crossed line, same exponential slope as in (d) with Campeche northern shelf and initial vortex north of the cape. (g) triangles, trajectory of the Loop Current ring in the MICOM simulation.

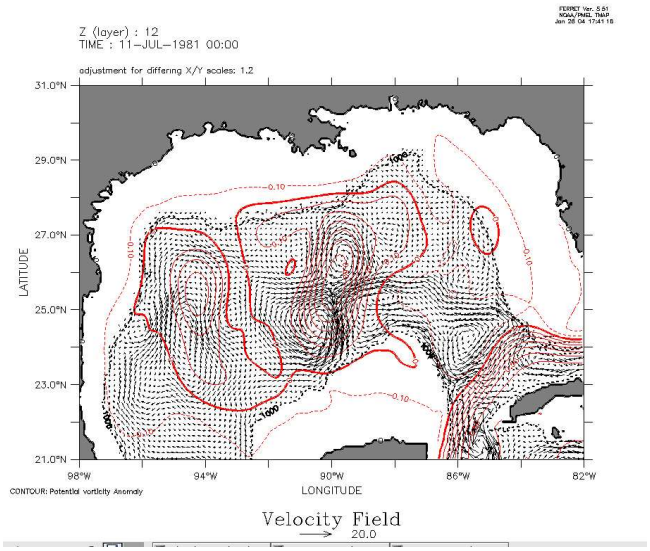

(a)

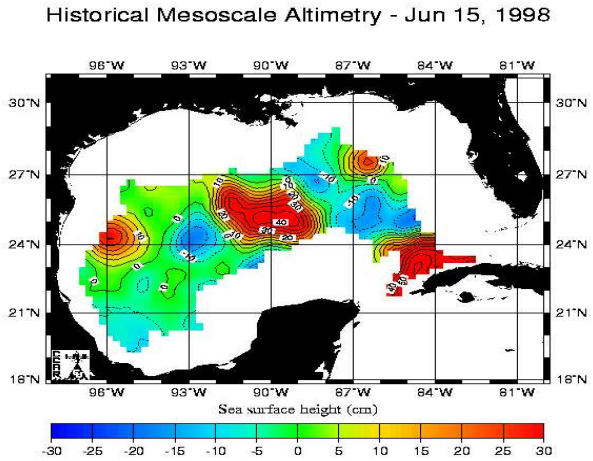

(b)

Figure 15: (a) Velocity field in layer 12 from the MICOM simulation, July 11, 1981. Red lines shows SSH contours. (b) SSH maps above waters deeper than 1500 m from the Real-time Altimetry project of Colorado Center for Astrodynamics Research, June 15 1998.

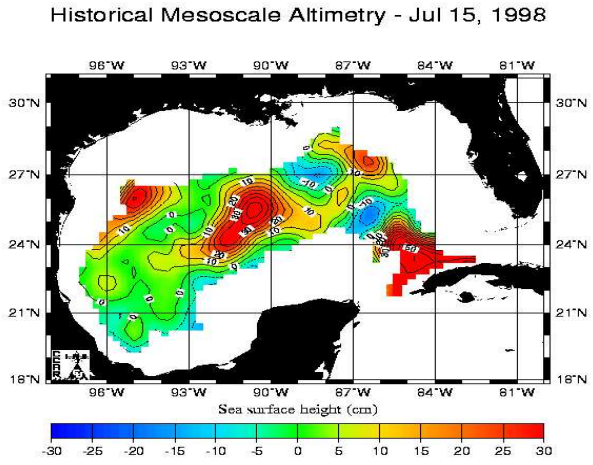

(a)

Figure 15: continued; (c) same as (b) on July 15, 1998.